NON INVASIVE APPROACH FOR THE DETECTION OF HUMAN ARTERIAL BLOCKAGES VIA PHOTO ACOUSTIC MODELLING

A Thesis

Submitted to the Faculty

of

Purdue University

by

Monika Kakani

In Partial Fulfillment of the

Requirements for the Degree

of

Master of Science in Electrical and Computer Engineering

December 2017

Purdue University

Indianapolis, Indiana

THE PURDUE UNIVERSITY GRADUATE SCHOOL
STATEMENT OF COMMITTEE APPROVAL

Dr. Maher Rizkalla, Chair

Department of Electrical and Computer Engineering

Dr. Paul Salama

Department of Electrical and Computer Engineering

Dr. Ahdy W.Helmy

Indiana University School of Medicine

Approved by:

Dr. Brian King

Head of the Graduate Program

I would like to dedicate this thesis work to my parents who have always supported me and motivated me throughout my studies and helped me face my challenges with courage. I also want to dedicate it to the rest of my family for always loving me unconditionally and helping me achieve everything I aspire to.

ACKNOWLEDGMENTS

I would like to express my gratitude to my professor Dr. Maher Rizkalla for supporting me throughout my thesis with his valuable suggestions. His immense knowledge and patience have helped me in all the research work and also in writing my thesis.

Besides my advisor, I would also like to thank my committee: Dr. Paul Salama and Dr. Ahdy Helmy for their suggestions, encouragement and tough questions.

I am very grateful to Dr. Brian King for extending me motivation and support for starting my masters degree at IUPUI. I would like to acknowledge INDI (Integrated Nano-systems Development Institute) lab for allowing use the software which was necessary for my research work. I would also like to thank Dr. Mangilal Agarwal for encouraging me throughout my master's.

Lastly, I would like to thank my parents and family for supporting me mentally and spiritually in being successful in my life.

TABLE OF CONTENTS

Page

Page

Page

LIST OF TABLES

LIST OF FIGURES

Figure Page

Figure Page

SYMBOLS

m	mass
v	velocity
Δ	delta
ω	frequency
T	temperature
ρ	density
c	speed
K	electrical conductivity
C	heat capacity
p	pressure

ABBREVIATIONS

LDL	Low Density Lipoprotein
HDL	High Density Lipoprotein
IVUS	Intra Vascular Ultra Sonography
VH-IVUS	Virtual Histology
NIRF	Near Infrared Fluorescence
MRI	Magnetic Resonance Imaging
CT	Computed Tomography
PET	Positron Emission Tomography
T.L	Transmission Line

ABSTRACT

Kakani, Monika. M.S.E.C.E., Purdue University, December 2017. Non Invasive Approach for the Detection of Human Arterial Blockages via Photo Acoustic Modelling. Major Professor: Rizkalla Maher.

This research focuses on the detection of arterial blockage due to LDL (low density lipoprotein). Arterial blockages are related to two kinds of fats LDL and the HDL. HDL being the good fat, the patient does not have to undergo the biopsy, while in case of LDL, biopsy should be performed. Issues associated with invasive approaches raise safety concerns for patients such as infection, longer operation durations, longer recovery time etc. This research focuses on a noninvasive imaging technique to detect the kind of block age. Photo acoustic approach was investigated in order to simulate human tissues leading to medical diagnosis and treatment. Photo acoustic imaging involves production of an image on absorption of laser pulses. The laser pulses are further scattered and absorbed producing heat. The goals of the study were to categorize the type of the tissue materials based on the output temperature distribution via IR sensors and reflected acoustic waves via acoustic pressure sensors. The reflected acoustic wave and IR thermal distribution may be applied towards arterial blockages to differentiate the different types of tissue layers. The simulation results should have implications towards the future implementation of the practical devices and system. Parameters including energy levels, tissue thicknesses, frequencies, penetration depth, and the densities of the LDL/HDL fat materials were considered. Various energy pulses; 1j, 3j, and 5j were considered as input sources to the tissue materials (single or multi layers). The simulated layers considered in the study were the skin, bone, blood, and fat cells.

The temperature and acoustic pressure response over the various layers were analyzed for the detection of blockages. The findings of the temperature and acoustic pressure ranges can be detected by MEMS/NEMS (Micro electro mechanical systems/nano electro mechanical systems) sensors, such as IR and Piezoelectric devices. Bioheat and acoustic wave equations were solved simultaneously using COMSOL software for multiple layers. The proper boundary conditions were provided in the solutions of these equations. The scattering and transmission acoustic wave, and the temperature distributions, may be used as guide to the integrated sensor system design for future consideration. The simulation was performed in four stages:

(1) Single layer and multiple layers at a given frequency and energy level

(2) Multiple layers at a given frequency for different energy levels

(3) Multiple layers at a given energy level for different frequency and

(4) Multiple layers at a given frequency and energy levels with different size tissues.

The simulation results showed that a range of acoustic pressure between 240 and 260 need to be detected, with a differential temperature distribution in kelvin range. Power pulses of 10MPa showed a temperature change of 175, which is believed to be within the flexible substrate sensing devices that may be used for the practical model of this research.

The thesis covers a proposed system for the practical model following the simulation results received in this study.

1. INTRODUCTION

1.1 Background

Medical imaging is a technique which visualizes the internal structures of the biological systems for the detection of abnormalities within human bodies. It generates data for signal processing and computer analysis that determines the status of a disease. These techniques involve methods such as electroencephalography (EEG), magnetoencephalography (MEG), electrocardiography (ECG), and computer tomography (CT).

Medical imaging techniques can be categorized into two different procedures: invasive and noninvasive imaging. Invasive techniques generally involves surgical procedures while noninvasive approaches provide safe imaging for diagnoses and treatment. There have been always limitations on the use of invasive procedures, giving features for the non-invasive techniques in many cases.

1.2 The Real Cause of Arterial Blockage

The coronary artery diseases is primarily because of the atherosclerosis, which is principally created because of the accumulation of lipids, white blood cells and cell debris inside the arterial walls. Atherosclerotic plaque enters the arteries causing the arterial clog. This leads to the limitation of blood flow inside the arteries which might rupture the arteries called as thrombosis or blood clotting. This condition completely blocks the flow of blood in the arteries.

Atherosclerosis is primarily linked with the cholesterol in a human body [1] as the atherosclerotic is due to the accumulation of the cholesterol [2]. Cholesterol in human body is a lipid with four hydrocarbon rings linked together with one hydrocarbon

group having a hydroxyl group as a tail and the other end linked to a steroid that does not get dissolved in the blood. The structure of the cholesterol is given in the Figure 1.1.

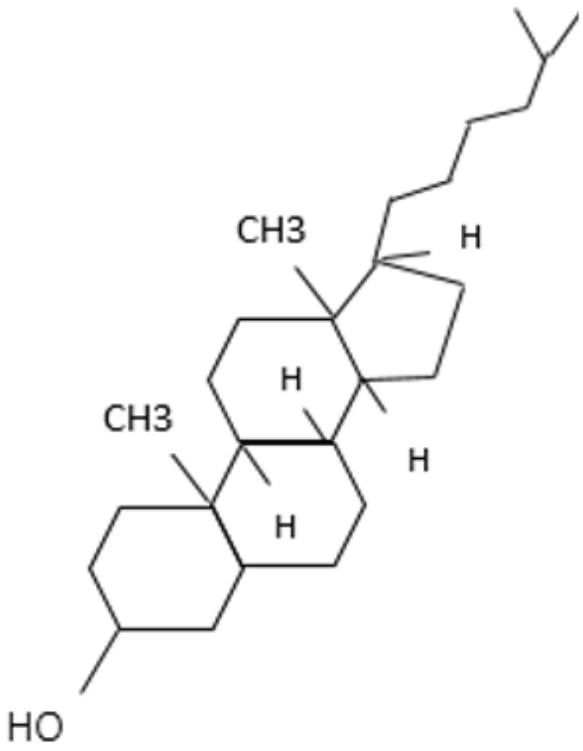

Fig. 1.1. Structure of cholesterol

About 80 % of the cholesterol is generated by the human liver while the rest comes from the diet from foods through animal products such as meats, poultry, fish and dairy products [3]. Cholesterol enables the synthesis of cell membrane, it acts as a precursor molecule, and produces hormones and vitamin D. Cholesterol has a very prominent role in human heart health as it can be both bad and good. Cholesterol cannot travel inside the blood stream and lipoproteins are used to transport the cholesterol inside the blood stream. Hence hydrophilic proteins are attached to the cholesterol forming a lipoprotein. Lipoproteins act as a transport agent that carries

various kinds of fats. Lipoproteins help the fats present inside the body to be transported to the required parts through receptor-mediated endocytosis [4][5]. Lipoproteins are built on multiple proteins each comprising of 80-100 proteins/particle. The level of cholesterol depends on how the lipoproteins are transported. So it is the accumulation of lipoproteins that cause the clog the arteries and not the cholesterol. The lipoproteins that cause the atherosclerosis are termed as atherogenic, and Apolipoprotein (apoB) is found to be the most important component of atherogenic lipoprotein [6]. Lipoproteins are classified into

1) Low density lipoprotein (LDL)

2) High density lipoprotein (HDL)

1.2.1 Low Density Lipoprotein

A single LDL fat molecule on average transports about 3,000 to 6000 depending upon the number of molecules present inside the fat and its size (around 220 to 275 angstroms) [7]. The size of the LDL varies because it consists of a number of fatty acids that keep changing in its number. An increase in the amount of LDL leads to the development of coronary heart disease [8]. LDL particles drive their particles into the arteries and these particles attract the macrophages thus leading to atherosclerosis.

Oxidized form of LDL results in cardiovascular diseases, as the proteoglycans retain the oxidized forms of LDL. The oxidized form of LDL is generated by the necrotic cell debris and free radicals present in the endothelium [9]. The LDL particles have a homogeneous structure. They have two different patterns; pattern A and pattern B. The latter is considered dangerous since they are smaller and denser in size and can penetrate easily through the endothelium. It has a size varying between 19.0 to 20.5nm, while pattern A has a size of 20.6-22nm [10].

The concentration of the LDL vary from a person to person due to their living style, day to day activity and hence the measurement of the LDL has certain diag-

nostic errors. Diagnostic errors occur when a single sample is analyzed many times. The errors occur due to the change in volume considered at the time of diagnosing or malfunctioning of the instrument or it also might be due to the formulation of reagent. Physiological errors occur even when the analytical errors are noticed to be zero and these are generally occurred when the individual is diagnosed more than once.

The NIH sponsored National Cholesterol Education Program (NCEP) Adult Treatment Panel III (APTIII) provides an overview of efforts to maintain the diagnosis and treatment of LDL in order to provide attention to the primary persons likely to have atherosclerotic diseases [11]. The LDL $<$ 1000 mg/l is considered as an optimal value while the ones with LDL $<$ 1300 mg/l are likely to be at high risk and LDL $<$ 1600 mg/l are considered to have no risk.

1.2.2 Estimation of Cholesterol

1.2.2.1 Blood Test

The most common way to check the LDL is through blood test. This technique generally reports what amount of low density lipoprotein is driving to cardiovascular diseases. It clinically calculates the percentage of cholesterol using a formula given from Friedewald equation [12][13]

$$L = C - H - KT, \tag{1.1}$$

H = HDL cholesterol, L = LDL cholesterol, C = total cholesterol, T= triglycerides and k = 0.20 when the quantities are measured in mg/dl and 0.45 when measured in mmol/l.

Limitations of Blood Test

The limitations of the blood test include

1) Samples must be obtained only after 12- 14 hrs of fast

2) The triglyceride should not be greater than 4.52 mmol/l

This technique has a great impact on finding out the concentration of the LDL particles and the size of the LDL particles rather than finding the percentage of cholesterol present in the blood. These results have proved that the greater the concentration of the LDL particles and smaller sized particles increases the risk of heart diseases [14].

1.2.2.2 Ultracentrifugation

This technique involves the separation of lipoproteins by adjusting the density of the specimen using salts such as NaBr or KBr [15] so that the particles float due to the difference in the densities [15]. The particles containing the LDL, HDL, IDL can be adjusted to 1.063 kg/l with the addition of KBr and then by processing it through ultracentrifugation [16] making the LDL float. This technique is observed to be very tedious and time consuming. It is also observed that this technique does not yield a proper output hence the other techniques are proposed.

1.2.2.3 Electrophoresis

Electrophoresis was a technique that was initially introduced by Fredrickson and Lees [17] which classifies the lipoprotein through their separation patterns. And then techniques such as cellulose acetate [18] and polyacrylamide [19] electrophoresis were introduced. Of all the techniques the one using agaros gels to separate lipoproteins and then this followed by precipitation with polyanions [20] and densitometric [21] scanning gave promising values [22-24].

1.2.3 High Density Lipoprotein (HDL)

HDL are tiny particles and are the smallest among all the lipoproteins. These are in the form of a rim usually containing 80-100 particles that mantle the cholesterol. These transport up to hundreds of fat molecule per particle and are considered to be denser than the other lipoproteins. HDL is considered to be an essential fat that stabilizes the body. HDL removes the LDL from the body by transporting it to the liver and it also heals the inner layers of the damages artery by scrubbing the walls of the artery. According to the epidemiological studies [25-36] have related that the high levels of HDL reduces the level of cardiovascular disease. A study conducted by the British Regional Heart Study (BRHS) proves that HDL does not lead to a significant risk to the coronary heart disease [37]. The cholesterol transported to the liver are excreted into the bile and then to the intestine after conversion into the bile acids. And hence HDL is sometimes referred as good cholesterol.

HDL is also transported to the adrenals, ovaries, and testes, and it is very important for the synthesis of the steroid hormones. The process of transporting the HDL cholesterol from the arteries to the liver until the conversion of bile acids is called reverse cholesterol transport. HDL particles contain lipids and proteins that are very low in concentrations but are very active. These particles enhance the ability of the HDL particles in protecting the person from atherosclerosis. Direct measurement techniques are considered to be expensive and hence HDL is tested using the blood tests. HDL is associated with the Apo-A and it carries around 30 % of the blood cholesterol along with the other fats [37]. HDL is also estimated in clinical laboratories through ultracentrifugation or chemical precipitation with the divalent ions such as $Mg^{+}2$ and then they are coupled with the products of cholesterol oxidase reaction to an indicator reaction and the reference method uses the combination of these two techniques [38].

These days the laboratories use analytical techniques in which the ApoB particles are blocked using the antibodies and then the colometric enzyme reaction is used to measure the non-blocked HDL particles [39]. Ultracentrifugation combined with electrophoresis is used to measure the HDL particles as they have net charge and vary by density and size.

1.3 Invasive Imaging

Invasive imaging techniques involve the invasion of a needle, tube, device, scope etc., into the body within major surgeries for medical diagnosis. Examples of invasive procedures include Coronary angiography, Intravascular Ultra Sonography (IVUS), Virtual Histology Intravascular Ultra Sonography (VH-IVUS), Integrated Backscattered Intravascular Ultra Sonography (IB-IVUS), (IMAP), and Coronary computed tomography angiography (CCTA). NIRS-IVUS, Coronary MRA being within the emerging techniques, and NIRF is considered within the investigation state. The details of these invasive procedures are given below.

1.3.1 Coronary Angiography

Coronary angiography is generally suggested by doctors when they suspect the blockage of the arteries with plaque, preventing the heart from getting pumped with oxygen. This technique induces a dye generally iodine and then x-ray imaging technique is used to detect the presence of plaque inside the coronary arteries. This technique is generally carried out through cardiac catheterization in which the surgeon first take x-ray images and chooses an appropriate place for the insertion of catheter into the body by making a hole. If the presence of plaque is detected the surgeon performs percutaneous coronary artery invention, which improves the flow of blood in the coronary arteries. Then the catheter is removed from the body.

The risks involves with coronary angiogram are very minor but is noticed to be risky for old aged people. The risks involved with it include heart attack, kidney damage, stroke, infection, excessive bleeding, etc., in some cases, the technique is not preferable, while it still been used if no other options are available.

1.3.2 IVUS (Intravascular Ultra Sonography)

The main advantage of this technique over angiography is that it can image the presence of plaque and is generally used to detect the amount of plaque present inside the arteries and stenosis (narrowing) of arteries. This technique involves the usage of a specially designed catheter with its distal tip attached to an ultrasound probe and the proximal end being attached to the ultrasound equipment. Angiographic techniques are used to view the artery or veins by placing the tip of the catheter guidewire steering it outside the body through angiographic catheter. Sound waves are emitted from the catheter tip ranging from 20-40 MHz and the ultrasound equipment constructs the image. The main disadvantages of this technique are related to the cost and the lengthy procedure in addition to the requirement of experts that are well trained.

1.3.3 VH-IVUS (Virtual Histology)

VH-IVUS provides a more detailed description of the composition of plaque (fibrous or fibrofatty), necrotic core and calcium density. It focuses on high radio frequency analysis of backscattered ultrasound signals [40]. This technique has refinements in IVUS improving the spatial resolution. This technique cannot be used to identify thrombus formation.

1.3.4 IB-IVUS

IB-IVUS is an algorithm developed by Kawasaki et al [41] which utilizes the time domain information from the radio frequency signal. This results in generating an improvised plaque characterization with a specificity of 92 % [42][43].

1.3.5 NIRF (Near Infrared Fluorescence)

This technique improves the potential and sensitivity of biological imaging [44] [45]. NIRF uses a source of photons generated by exciting light within a defined bandwidth (650-900nm). When the photons are collided by optical agent or the fluorescent probe fluorescence is emitted into the NIR window. The emitted fluorescence is detected by filter and high charge coupled camera. The main drawback of this technique is that provides compositional information but does not provide any details regarding structural information.

1.3.6 IMAP

IMAP is a type of IVUS technique developed using pattern recognition of radio frequency signals [46][47][48][49]. IMAP technique uses a different algorithm for imaging system with signal trigger is utilized.

IMAP imaging has some disadvantages. It cannot display gray scale images clearly. The resolution of the images produced by IMAP imaging are high but they have rotational distortion. It is also problematic as it needs high frequency catheters that may backscatter the blood.

1.3.7 Summary of the Limitations of Invasive Techniques

There are still a number of drawbacks that limit the use of invasive techniques. The following covers some of the concerns of these techniques

1) Longer time for operation

2) Might lead to open surgery

3) Difficulty in handling the equipment

4) Risk of infection

5) Long time of recovery

6) Soars and wounds on the body

1.3.8 Issues with Invasive Approach

In addition to the above mentioned limitations for the invasive procedures, there are still other issues that the physicians should consider within the procedures.

1) The surgeons should be aware of the emerging technologies including the equipment being used for the imaging as the invasive technique invades inside the human body through catheter, needles, etc

2) The coronary angiography at times might lead to the infection with cytomegalo virus or chlamydia pneumoniae

3) Includes the incidence of cerebral emboli

4) Must be careful with lethal complications

5) These techniques do not prevent scarring

1.4 Non-Invasive Imaging

Non-Invasive imaging is a technique used to image the internal parts of human body without involving any surgical process. Examples of non-invasive imaging are Radiography, magnetic resonance imaging (MRI), computed tomography (CT), Ultrasound or medical ultrasonography, thermography, Positron Emission Tomography (PET), and Photo Acoustic Imaging.

1.4.1 Radiography

Radiographic imaging is a 2D imaging technique and it is mainly classified into projection radiography and fluoroscopy. Projection radiography is mainly known as x-rays and it is used to detect the type of fracture and to what extent the bones are fractured. It is also used to detect the pathological changes in the lungs and visualize the structure of intestines and stomach. It is mainly used to diagnose the ulcers. Fluoroscopy uses a constant input of x-rays at a lower dose. It is used to generate the real time images of the internal structures of the body. It requires and image receptor to convert the radiation into image. The main limitations of this technique are cost of devices, cost of converting previous records to digital, learning to use the concept, thickness of the sensor, rigidity of the sensor, and loss or breakage of the sensor.

1.4.2 Magnetic Resonance Imaging (MRI)

MRI technique uses high field strength magnets and radio frequency pulses through which the hydrogen nuclei of the water molecule are excited producing a signal to be encoded. The encoded signal generates the images of the body. At times the technique requires an intravenous dye to show the images clearly. This technique is mainly used to image brains, pelvis (uterus/ovaries), abdominal area and breast. The limitations of MRI scanning is the magnetic field generated by MRI scanner attracts any metal objects, it can also pull any metal containing objects inside the body such as medicine pumps, aneurysm clips, medical implants get heated up during the scan. MRI scanners might cause the malfunction of heart pacemakers, defibrillation devices and cochlear implants.

1.4.3 Computed Tomography (CT)

Computed Tomography uses rotating X-rays to generate the images of the body which are exquisitely in detail. In this technique the x-rays are blocked by a tissue

to create an image in which the soft tissues are poor in quality. This technique suggests the patient to consume liquids prior to the scan. As this would help in better evaluation of the intestines. The limitations of CT scan include the artefact, CT scan of brain affects the nearby bones. This technique needs a person to hold his breathe which is unmanageable by patients. Involves high dosage of radiation.

1.4.4 Ultrasound or Medical Ultrasonography

Ultrasound imaging using very high frequency sound waves to produce 3D images. The sound waves are sent to tissue and the signals are attenuated and returned at separate intervals. The waves are then sent to the transducer to generate the images. This technique is generally used to image fetus in pregnant women. Limitations of ultrasound includes the detection of nonmalignant area because of which a biopsy might be recommended. Many cancers cannot be detected. These are not available all around the world and insurances generally do not cover them. It requires highly skilled operator to detect malignant lumps.

1.4.5 Positron Emission Tomography (PET)

PET is a nuclear imaging technique used to detect the functioning of organs and tissues. It is often combined with CT imaging, a scanner, and radio pharmaceuticals. These are injected to the patient's vein for a detailed image of the organs inside the body. It is generally used to detect Alzheimer's, multiple sclerosis, cancer, heart conditions. The limitations of this technique are the radioactive materials used in this process might not be suitable for every patient. A patient can undergo a PET scan only a limited number of times. It is expensive and it is not offered in majority of the medical centers.

1.5 Photo Acoustic Imaging

Biomedical applications using photo acoustic imaging has come a long way in the last decade [49-53]. Photo acoustic imaging also called as opto acoustic imaging is a noninvasive imaging technique. This technique uses short EM pulses converted into EM energy acts as a source. The delivered energy is absorbed by the tissues with time delays and it is converted into heat. This leads to transient thermos elastic expansion and this leads to wide band ultrasonic emission. The generated ultrasonic waves are detected by the transducers and then the images are generated.

The spatial resolution and the maximum imaging depth of the photo acoustic images can be manipulated with the ultrasonic bandwidth [54]. Spatial resolution of 1mm can be produced by the signals with a bandwidth of 1 MHZ while the bandwidth being increased to 10MHz produces a spatial resolution of 0.1mm which helps in ultrasonic penetration. PA depth profiling is a PA imaging technique where we can determine the depth structure and properties of a sample. This technique utilizes a wide beam of light pulses heated over a layered medium. The light pulses are converted into energy and PA energy is spread throughout the depth of the sample. To determine the properties of complex structures we use a method called PA tomography (PAT), and also called opto acoustic tomography(OAT) referring to light induced PA or thermos acoustic tomography (TAT) referring to RF-induced PAT. This technique studies the sample by measuring various locations around the sample.

1.5.1 Features of Photo Acoustic Imaging Versus Ultrasound

The factors affecting the spatial fidelity and resolution are same for both the imaging techniques but the sources used are different. An ultra sound image represents the acoustic impedance mismatch between the different tissues hence focusing on mechanical and elastic properties while the photo acoustic imaging focuses on initial pressure distribution generated due to optical energy.

Photo acoustic imaging has a greater differentiation and specificity when compared ultra sound imaging due to its differences in optical absorption between the tissues. PA imaging has strong optical absorption for the hemoglobin making it suitable for the micro vasculature.

1.5.2 Features of PA Versus other Optical Approaches

Optical imaging is a non-invasive imaging technique that uses visible light along with the special properties of photons for producing the detailed images of organs. This technique protects the patients from getting exposed to harmful radiation, specially used for soft tissue imaging. Optical imaging has various techniques such as endoscopy, optical coherence tomography, photo acoustic imaging, and diffused optical tomography. Patient's internal organs are imaged by sending a flexible tube into the human body through the patients mouth. Optical coherence tomography, a medical imaging technique which uses light is used to produce the sub surface images. Diffuse optical tomography is used to generate the information related to brain using near infrared laser. Photo acoustic imaging uses laser pulses to generate the images. Scattering of photo acoustic imaging is weaker when compared to the optical imaging while the spatial resolution of the photo acoustic signals is high and has a depth greater than 1mm [55].

1.5.3 Photo Acoustic Versus Infrared (Thermal/Acoustic wave generation)

Imaging through infrared rays is called as thermography and it detects radiation in the long infrared rays. The images produced by thermography are called as thermograms. Infrared rays are generally emitted by black body objects hence it is possible to see the environment even in invisible light and it can detect the physiological changes many years prior. Thermography uses infrared detectors for the detection of heat and increased vascularity. Thermography cannot suspect the exact location

of the suspected area but it can be used as a functional testing.

Photo acoustic imaging is a structural imaging and it detects the pinpoint location of the suspicious or effected area. This technique uses high frequency sound waves that are bounced back by the affected area and are further collected as echoes in order to produce the images. These are good to distinguish between solid and fluids tissues.

1.6 Research Hypothesis

The emphasis of this work concentrates on the photo acoustic study. Photo acoustic waves may come in the form of LASER ENERGY applied to multiple layered structures within the human subjects. The study presented here targets non-invasive approach for detecting the blockages of the human arterial system. The LDL (low density lipoprotein) fat material present inside the arterial are usually the cause of the blood clot leading to heart attacks. Therefore, the emphasis of this work concentrates on means of detecting this type of material. This medical imaging approach using photo acoustics is in efforts to a non-invasive approach for detecting the LDL fat material inside the human arteries.

Photo acoustic imaging as optical imaging combined with acoustic imaging features high spatial resolution and high contrast. Photo acoustic image can be produced by inducing laser pulse onto the tissue surface and depth of penetration depends upon the wavelength of the induced light. The induced laser pulse beams are scattered and absorbed, and converted into heat. This heat pulse is received by the ultrasound receiver and the PA image is formed from the received heat pulses.

Maximum permissible exposure (MPE) is the rate at which a person can be exposed to the EM radiation without causing any changes or damaging the tissues [56]. If tissues are exposed beyond the MPE value it might result in destroying the tissues. The value of the MPE depends upon the length of the wave and the duration for which the body is exposed to the wave. The MPE is less when the duration is longer

and it is greater if the wavelength is greater. The American national standards has specified the different MPE levels for the specific exposure time and wavelengths [47]. These studies have proved that the photo acoustic rays do not break the biological tissues or cause any damage to the tissues. These rays use only non-ionizing radiation and quantifies the oxygenation of hemoglobin [56]. Hence it is ideal for the in vivo applications.

Photo acoustic imaging has found a wide range of applications in the field of medicine, biology and clinical assessment that assist diagnosis in cardiovascular diseases, cancer etc. Figure 1.2 indicates the relation between the acoustic and thermal energy generated from the photo acoustic source applied to the human tissue.

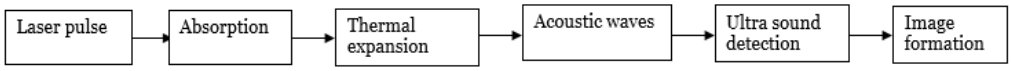

Fig. 1.2. Block diagram of photo acoustic imaging

In this thesis, the Photo acoustic approach was considered as a non-invasive approach for the determination of the type of arterial human blockages, considering the research parameters impacting the final PA images from the human arterial system.

Chapter 2 details the photo acoustic imaging approach, features and limitations. The mathematical models and the physics are given in chapter 3. Chapter 4 discusses the results of simulation for the single and multiple layers. Chapter 5 details the proposed hardware devices with flexible substrates that are suitable for the practical model of the project. Chapter 6 gives the conclusion and future work.

2. PHOTO ACOUSTIC IMAGING

2.1 Introduction

Evolution of photo acoustic imaging is based on the photo acoustic effect, generation of the acoustic wave with the absorption of the electromagnetic energy i.e. the optical or the RF energy [56]. PA has come a long way from the time it has been discovered as a sound wave by Alexander graham bell in 1880 [57] and found its application in various fields [58-62]. It has marked its impact in biological imaging since a decade [38-43]. PA imaging is considered as an EM enhanced ultrasound. The tissue absorbs the incident EM wave and then it converts the EM energy into the heat energy via thermal expansion. These waves are further received by the ultrasound receivers and are then mapped for the absorption properties.

The energy used for generating the acoustic waves are generally the electromagnetic waves in the optical and the RF regions. It has been studied that the waves between these regions is not only considered to be safe for the human body but also provide great penetration depths [63-67]. Radiations such as ultraviolet rays have greater photon energy and hence they are considered to be harmful for human body. The optical properties i.e. the absorption and the scattering patterns of the biological tissues in the visible region and near IR region are related to the vibrational structures of the tissues. The scattering in the biological tissues is pretty strong and it is described by the scattering coefficient which is equal to 100 cm-1 in the visible to near IR region [64] and the absorption coefficient can be increased by adding the agents such as indocyanine green [56].

The light scattering inside the tissues follows diffusion law providing high resolution images. While the RF properties are related to the physiological properties of the tissue electrical properties and they are related by the complex of electrical permittivity or complex conductivity. EM waves in this region are readily absorbed, transmitted or reflected by the biological tissues but a little scattering occurs at this range [66].

2.2 Photo Acoustic Generation

There are many imaging techniques that exist but we are interested in imaging the biological tissues using the EM waves in between the visible region and near IR region. The EM waves uses the thermoelastic mechanism to excite the transient ultrasonic waves through low fluence EM radiation. The thermoelastic mechanism produces the sound wave due to a slight increase in the temperature caused by the absorption of EM the energy inside the biological tissues. In order to generate the acoustic waves effectively two main conditions namely thermal and stress confinements should be met [68]. The amount of heat dissipated due to the thermal conduction can be given by T_{th}

$$T_{th} = \frac{l^2{}_p}{4D_T} \tag{2.1}$$

Where $l^2{}_{\mathrm{p}}$ the characteristic is linear dimension of the tissue volume being heated and D_{T} is the thermal diffusivity and its typical value for tissues is 1.4 x 10-3 cm2/s. The diffusion of the heat depends on the volume of the geometry that absorbs the heat and T_{th} may vary [69]. The diffusion length of the energy upon the absorption of the pulse for a temporal time can be estimated by

$$\delta_T = 2^2\sqrt{D_T T_p} \tag{2.2}$$

The value of T_p is expected to be smaller than the T_{th} for efficient PA wave generation and this condition is referred as thermal confinement i.e. the heat diffused during the excitation of the pulse is negligible. The time for the stress to be transited to the heated region can be given by

$$T_s = \frac{l_p}{c} \tag{2.3}$$

Where c is the speed of the sound and it is expected to have a shorter T_p than T_s and this condition is called as stress confinement. When both the stress confinement and the thermal confinement are met there would be an increase in a pressure p_0 and this can be estimated by [68] [70]

$$p_0 = \frac{\beta C^2}{C_p \mu_a F} = \Gamma A \tag{2.4}$$

Where β is the isobaric volume expansion coefficient $K^{-}1$, C_p is the specific heat in $\frac{J}{(Kg)}$, μ_a is the absorption coefficient in $cm^{-}1$, F is the local light fluence in $\frac{J}{cm^2}$, A is the local energy deposition density in $\frac{J}{cm^3}$: A= μ_a F and Γ is referred to as gruneisen coefficient,which relates the intial pressure p_0 to the absorption co-efficient expressed as Γ=$\frac{\beta C^2}{C_\mathrm{p}}$ [56].

The excited EM pulse pressure acts as a source propagating the acoustic waves in 3 dimensional space. The speed of the sound inside the tissues remains constant at 1.5 mm/ s [63][64]. The scattering properties of the tissues and the depth penetration of the waves are considered to be low for lower frequencies [63][64]. The energy lost due to both the absorption and scattering are given by the total attenuation which is temperature and frequency dependent. The frequency dependency of the total attenuation can be expressed by the equation [56]

$$\mu = aF^b \tag{2.5}$$

Where μ is the ultrasonic attenuation coefficient, a and b being the constants and f is the ultrasound frequency [63]. The attenuation is expected to be increased with the increase in frequency while the penetration depth decreases with the increase in

frequency. The acoustic waves from the source are applied to the tissues and the waves from the tissues are collected by the transducer. The information provided here may assist the practical model of the project. The transducers designed are piezoelectric based due to its marked advantages [69]. Sensors based on optical detection can also be chosen [65-71] and these are often based on photo acoustic pressured induced surface displacement [65][66][70] or refractive index [67] i.e. they can measure non contact (measurement device doesńt have to touch physically) and large areas [68]. The initial pressure distribution generated in response to a wide impulse pulse is given in Figure 2.1.

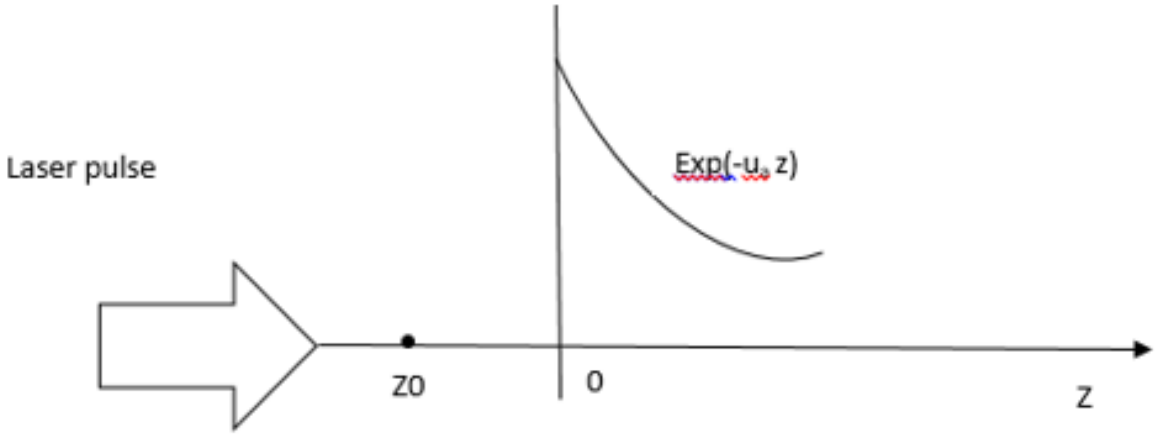

Fig. 2.1. Initial pressure distribution [56]

2.3 Scanning Tomography

PA scanning tomography is considered to be similar to the B-mode(brightness mode or 2D mode) ultrasonography [56]. The tissue surface is scanned by an focused ultrasonic transducer which itself converts the electrical energy into thermal energy and the each detected signal is converted into the 1D image across the axis. All the

images that are obtained from various positions on the same plane produce images. The axial resolution of the image depends upon both the width of the radiation pulse and impulse pulse of the transducer [56]. The lateral resolution depends upon the focal diameter of the transducer and the center frequency of the received PA signals and imaging zone depends on the focal zone of the transducer [76] as the image resolution decreases greatly beyond the focal zone. Figure 2.2 shows the diagram of thermoelastic scanning tomography.

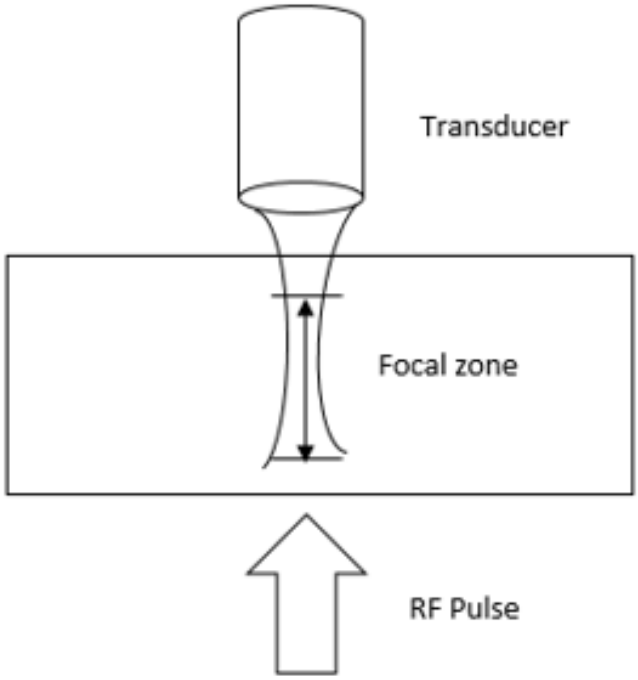

Fig. 2.2. Thermoelastic scanning tomography [56]

2.4 RF Scanned Tomography

RF induced PA imaging can be done by scanning the focused ultrasonic transducer [71-73]. The bandwidth of the PA signal is expected to be the reciprocal of the EM pulse width and hence a milli sec duration pulse of the RF signal can excite up to a several megahertz [56] providing a spatial resolution in milli or sub milli meters for centimeter thick tissue. This technique is used when the depth of penetration is expected to be large [56]. Figure 2.3 represents the ultrasonic transducer.

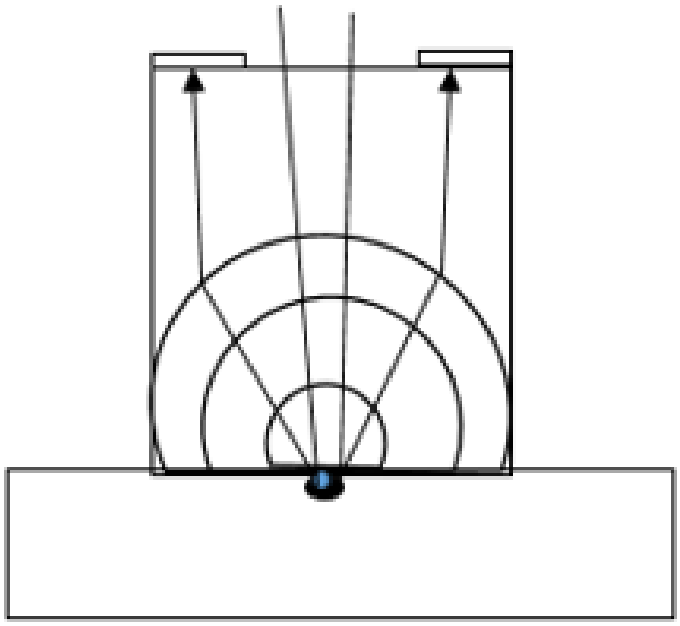

Fig. 2.3. Ultrasonic transducer [56]

2.5 Laser Based Microscopic Imaging

Laser based microscopic imaging is very similar to the RF based imaging but this technique scales down the image to microscopic range [74]. The laser pulses can generate an energy of 100mJ in less than 10ns and keep the ability to excite the PA signals of 100MHZ or greater frequencies keeping the axial resolution of 30m or less. This provides it the ability to imaging the skin and other delicate organs [56]. This technique is noticed to have an advantage over the other imaging techniques due to their high resolution images. Figure 2.4 shows the acoustic lens of focal length f.

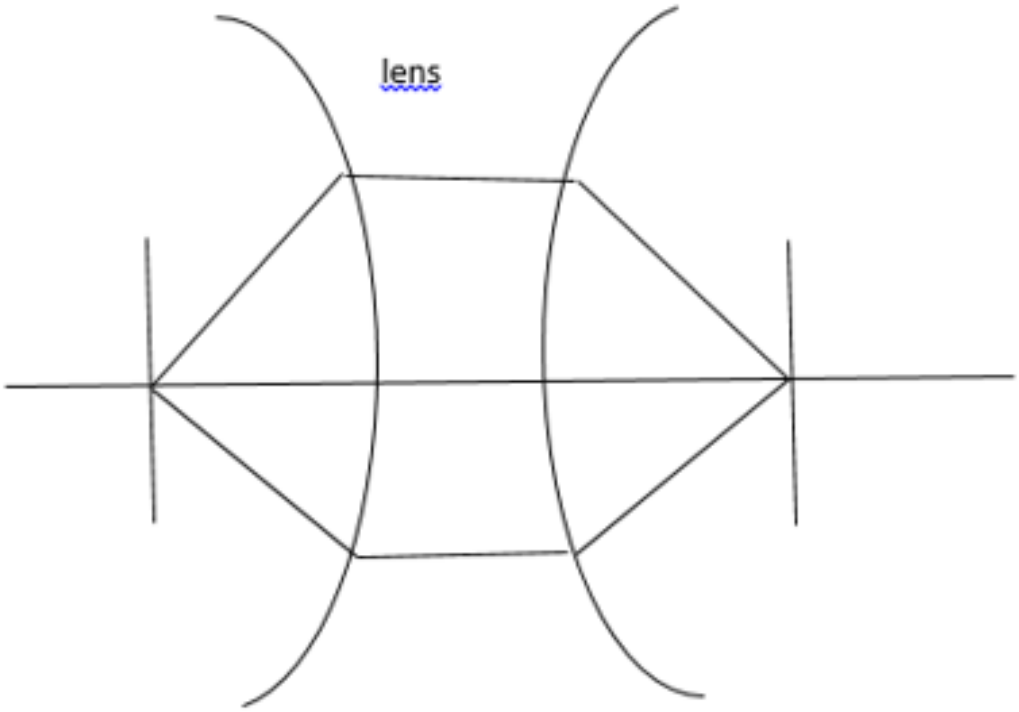

Fig. 2.4. Acoustic lens of focal length f [56]

2.6 Means of Simulation

In order to approximate the size and shape of the particle a numerical method called as FEM can be utilized. This technique reveals the physical information of the particle by providing the details of the individual spatial points of the cells. This technique uses spherical waves for the simulation. Apart from this technique cytometric techniques are also invented [56]. This technique is used to assess the morphology of the cells and in large number.

3. ACOUSTIC AND THERMAL POWER TRANSMISSION THEORY

3.1 Introduction

Due to the separation between the layers in between the multilayered structures the delaminations are detrimental to the mechanical and electrical properties. This is due to the mismatch caused between the layers as a result of the thermal stress [75]. Conventional techniques utilize the time delay established between the reflected waves to construct the image but the usage if this technique is limited [76].This technique has a limitation in its resolution. The waves are reflected only when the size of the defect is greater or comparable to the wave length. Smaller defect size results in scattered waves and the smaller wavelength waves are not deep enough to penetration [76].

3.2 T.L Modeling

Two different waves are produced when a plane wave meets at the interface of different materials transmitted wave and the reflected wave [76]. Reflections and refractions are observed when the ultrasonic wave travels through the sublayers of these multiple materials and the acoustic properties of these materials change the amplitude of the outgoing wave [76]. The transfer matrix technique is used to analyze the ultrasonic technique. Consider and incident wave given by the equation 3.1

$$u_{\mathrm{I}} = Ae^{i\omega t - k_1 x} \tag{3.1}$$

equation 3.2 and 3.3 represents the transmitted wave and the reflected wave

$$u_{\mathrm{T}} = Ae^{i\omega t - k_2 x} \tag{3.2}$$

$$u_{\mathrm{R}} = A_{\mathrm{R}} e^{i\omega t + k_1 x} \tag{3.3}$$

Equation 3.4 and 3.5 represents the combined wave equation in medium 1 and 2

$$u_1 = A e^{i\omega t - k_2 x} + A_{\mathrm{R}} e^{i(omegat + k_1 x} \tag{3.4}$$

$$u_2 = A_{\mathrm{T}} e^{i\omega t - k_2 x} \tag{3.5}$$

Applying the principles of continuity of pressure and particle velocity we get the equations 3.6 and 3.7

$$A + A_{\mathrm{R}} = A_{\mathrm{T}} \tag{3.6}$$

$$\rho_1 v_1 (1 - a_{\mathrm{R}}) = \rho_2 v_2 a_{\mathrm{T}} \tag{3.7}$$

solving the equations 3.4 and 3.7 we get

$$A_{\mathrm{T}} = \frac{2\rho_1 v_1}{\rho_1 v_1 + \rho_2 v_2} A \tag{3.8}$$

$$A_{\mathrm{R}} = \frac{\rho_1 v_1 - \rho_2 v_2}{\rho_1 v_1 + \rho_2 v_2} A \tag{3.9}$$

We can express the stresses produced by the incident, transmitted and reflected waves by the equation 3.10, 3.11, 3.12

$$\delta_{\mathrm{I}} = i k_1 (\lambda_1 + 2k_1) e^{i\omega t - k_1 x} \tag{3.10}$$

$$\delta_{\mathrm{T}} = i k_1 (\lambda_2 + 2k_2) e^{i\omega t - k_2 x} \tag{3.11}$$

$$\delta_{\mathrm{R}} = -i k_1 (\lambda_2 + 2k_2) e^{-} i\omega t - k_1 x \tag{3.12}$$

λ here denotes the wavelength and K denotes the longitudinal elastic stiffness coefficient

Deriving the transmission and reflection coefficients we get

$$T = \frac{(\lambda_2 + 2k_2)A_{\mathrm{T}}}{(\lambda_1 + 2k_1)A} = -\frac{2\rho_2 v_2}{\rho_1 v_1 + \rho_2 v_2} \tag{3.13}$$

$$R = \frac{A_{\mathrm{R}}}{A} = -\frac{\rho_2 v_2 - \rho_1 v_1}{\rho_1 v_1 + \rho_2 v_2} \tag{3.14}$$

The intensity coefficients are given by

$$T_1 = \frac{\frac{4\rho_2 v_2}{\rho_1 v_1}}{(\frac{\rho_2 v_2}{\rho_1 v_1} + 1)^2} \tag{3.15}$$

$$R_1 = (\frac{\frac{4\rho_2 v_2}{\rho_1 v_1} - 1}{\frac{\rho_2 v_2}{\rho_1 v_1} + 1})^2 \tag{3.16}$$

3.3 Derivation of T-matrix

Figure 3.1 shows the multilayer structure. Let us consider a continuous longitudinal wave y(x,t) entering from the left side x=0 and they enters the first layer. Equation 3.17 represents the wave equation after the wave has reached the steady state.

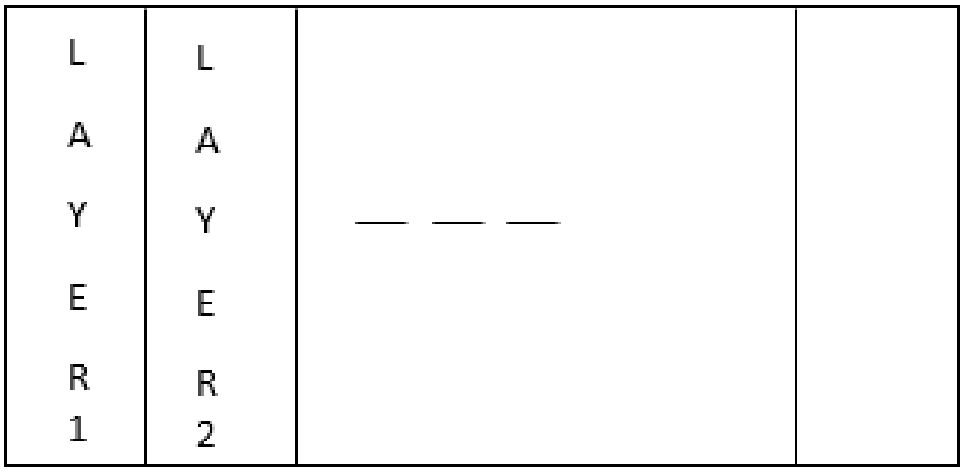

Fig. 3.1. Illustration of Multilayer structure

$$y_1 = A_1 e^{i\omega t - k_1 x} + B_1 e^{i\omega t + k_1 x} \tag{3.17}$$

similarly for the $m^t h$ layer

$$y_{\mathrm{m}} = A_1 e^{i(\omega t - k_{\mathrm{m}} x)} + B_1 e^{i(\omega t + k_{\mathrm{m}} x)} \tag{3.18}$$

ω here represents the angular frequency and and the wave number is given by k_{n}

$$k_{\mathrm{n}} = \frac{\omega}{v_{\mathrm{n}}} \tag{3.19}$$

By applying the conditions of continuity and normal particle velocity e can derive the relationship between various coefficients at the $n^t h$ cell

$$A_{\mathrm{n+1}} + B_{\mathrm{n+1}} = A_{\mathrm{n}} e^{ik_{\mathrm{n}} a} + B_{\mathrm{n}} e^{ik_{\mathrm{n}} a} \tag{3.20}$$

$$Z_{\mathrm{n+1}} A_{\mathrm{n+1}} - Z_{\mathrm{n+1}} B_{\mathrm{n+1}} = Z_{\mathrm{n}} C_{\mathrm{n}} e^{ik_{\mathrm{n}} a} + Z_{\mathrm{n}} D_{\mathrm{n}} e^{-ik_{\mathrm{n}} a} \tag{3.21}$$

The acoustic impedance of the material inside the each layer can be given by the equation 3.22

$$z_{\mathrm{n}} = \rho v_{\mathrm{n}} \tag{3.22}$$

From the equations 3.20 and 3.21, we can derive the matrix

$$\begin{pmatrix} A_{\mathrm{n}} \\ B_{\mathrm{n}} \end{pmatrix} = \frac{1}{2Z_{\mathrm{n}}} \begin{pmatrix} (Z_{\mathrm{n}} + Z_{\mathrm{n+1}})e^{ik_{\mathrm{n}}d_{\mathrm{n}}} & (Z_{\mathrm{n}} - Z_{\mathrm{n+1}})e^{-}ik_{\mathrm{n}}d_{\mathrm{n}} \\ (Z_{\mathrm{n}} - Z_{\mathrm{n+1}})e^{ik_{\mathrm{n}}d_{\mathrm{n}}} & (Z_{\mathrm{n}} + Z_{\mathrm{n+1}})e^{-}ik_{\mathrm{n}}d_{\mathrm{n}} \end{pmatrix} \begin{pmatrix} A_{\mathrm{n+1}} \\ B_{\mathrm{n+1}} \end{pmatrix} \tag{3.23}$$

$$= T_{\mathrm{d_n}} \begin{pmatrix} A_{\mathrm{n+1}} \\ B_{\mathrm{n+1}} \end{pmatrix}$$

Similarly we can derive the matrix by observing the transmission and reflection between the $(n+1)^t h$ ans $(n+2)^t h$ layers

$$\begin{pmatrix} A_{\mathrm{n+1}} \\ B_{\mathrm{n+1}} \end{pmatrix} = \frac{1}{2Z_{\mathrm{n+1}}} \begin{pmatrix} (Z_{\mathrm{n+1}} + Z_{\mathrm{n+2}})e^{ik_{\mathrm{n+1}}d_{\mathrm{n+1}}} & (Z_{\mathrm{n+1}} - Z_{\mathrm{n+2}})e^{-}ik_{\mathrm{n+1}}d_{\mathrm{n+1}} \\ (Z_{\mathrm{n+!}} - Z_{\mathrm{n+2}})e^{ik_{\mathrm{n+1}}d_{\mathrm{n+1}}} & (Z_{\mathrm{n+1}} + Z_{\mathrm{n+2}})e^{-}ik_{\mathrm{n+1}}d_{\mathrm{n+1}} \end{pmatrix} \begin{pmatrix} A_{\mathrm{n+2}} \\ B_{\mathrm{n+2}} \end{pmatrix} \tag{3.24}$$

$$= T_{\mathrm{d_{n+1}}} \begin{pmatrix} A_{\mathrm{n+2}} \\ B_{\mathrm{n+2}} \end{pmatrix}$$

With relevance to the 3.23 and 3.24 we get

$$\begin{pmatrix} A_{\mathrm{n}} \\ B_{\mathrm{n}} \end{pmatrix} = [T_{\mathrm{d_n}}][T_{\mathrm{d_{n+1}}}] \begin{pmatrix} A_{\mathrm{n+2}} \\ B_{\mathrm{n+2}} \end{pmatrix} \tag{3.25}$$

From equation 3.25 we can get

$$\begin{pmatrix} A_1 \\ B_1 \end{pmatrix} = [T(m)] \begin{pmatrix} A_{\mathrm{m+1}} \\ B_{\mathrm{m+1}} \end{pmatrix} \tag{3.26}$$

where [T(m)]= $[\mathrm{T_{d_1}}][\mathrm{T_{d_2}}][\mathrm{T_{d_3}}].....[\mathrm{T_{d_{m-1}}}][\mathrm{T_{d_m}}]$

3.4 Impedance Matching

The ultrasonic waves are longitudinal in nature [77]. These ultrasonic waves are sent into the human body through matched multi layers. The medium tends to act like a refractive medium when the adjacent particles start moving away from each other and it acts like a compressive medium when they move towards each other. The focus point and the direction of the wave can be adjusted by the phased array

technique [76]. The speed of the sounds depends on the density and stiffness of the medium.A partial reflection can be seen at the boundaries of the human tissues having a change in the acoustic impedance. These reflected waves are further collected to form an image by the transducer.

Though a lot of research have been performed on piezoelectric materials, medical imaging transducer using the matching layer has not gained a lot of attention. In order to achieve high sensitivity the quarter wavelength between the matching layers and imaging medium are very important. This is because waves can not be sent into the human body if there is a lot of difference between the piezo electric material and the transducer [78]. If proper matching is not attained, acoustic impedance mismatch will cause 80% of the ultrasound energy to reflect at the interface of the resonator and the human tissue [79].In order to design a lossy backing layer transducer, theoritically the acoustic impedance(z_{m}) should be the geometric mean of the piezoelectric material(z_{p}) and imaging tissue(z_{t})

$$(z_{\mathrm{m}}) = \sqrt[2]{(z_{\mathrm{p}})(z_{\mathrm{t}})} \tag{3.27}$$

3.4.1 Principle of Quarter Wavelength Matching Layer

The ultrasonic wave transmission is improved by establishing a matching layer in between the target medium and the front face of the piezoelectric material [76]. The best impedance matching can be achieved when the thickness of the matching layer is quarter wavelength of the transducer operating frequency. Sensitivity of the system is further improved by choosing an appropriate material with proper acoustic impedance. In order to analyze the acoustic impedance of the system, transmission matrix technique can be used [81].

3.5 Physical Parameters that May Impact the Multilayer Matching

Ideal multilayer matching is difficult to achieve due to its dependency on the bandwidth [82]. The transducer bandwidth gets wider with the double layer structure [83][84][85][86] and this can be achieved by using a sequential quarter wavelength layers with higher impedance material adjacent to the piezoelectric material and the lower impedance material facing outwards direction. In order to make a practical transducer with sufficient bandwidth leads to a reduction in the transducer sensitivity [87]. Precise thickness control is necessary in order to obtain proper matching between the layers. It is not simple as the thin layers need high frequency designs. Another major problem faced by the designers is choosing the composite materials and predicting their material performance. One can determine the mixture ratio, particle material, size distribution by experimental trial and error method for every case.

4. GOVERNING EQUATIONS AND SIMULATION MODELS

COMSOL Multiphysics software has been used to model the device. The software allows to integrate the geometry designed from various other CAD software. It allows us to couple the multiple physics and also to enter the coupled partial differential equations. The software has several modules categorized according to the area of applications like electrical, chemical, mechanical, fluid, etc. The COMSOL Multiphysics simulations can be interfaced with the CAD packages, MATLAB and Excel. COMSOL is an easy to use software for modeling and simulating in the real world multiphysics stream.

4.1 Models used for Modeling the Device

The modeled device needs to be integrated with the laser pulses and the heat transfer. Hence this study uses the pressure acoustics from the acoustic physics and bio heat transfer for the spreading the heat uniformly inside the tissues.

4.1.1 Acoustic Module

The acoustic model is used for designing the devices that use the acoustic waves or that produce the acoustic waves that are to be measured. This module consists of interfaces that are enabled to measure the propagation of sound in fluids and solids. Classic problems such as scattering, diffraction, emission, radiation and transmission of sound can be easily modeled using the pressure acoustics model. The pressure acoustics module enables us to solve the stationary pressure in frequency domain where the Helmholtz equation solved or as transient system where the classical scalar

wave equation is solved. Acoustic model has many options for boundary conditions such as boundary condition for a wall or an impedance condition for porous layer. Radiation or floquet boundary conditions can be used to model the open or periodic boundaries.

4.1.2 Heat Transfer Module

The heat transfer module helps in investigating the effect of heating and cooling inside the devices. The model consists of tools for conduction, convection and radiation. It acts as a context for all the industries where the applications rely on the creation, consumption or transfer of heat energy. The interfaced module bio heat transfer is used for this model. It is the perfect model for the human tissues and the biological systems through heating with microwave or resistive or chemical or radiative heating. This model could be combined with a variety of phase change phenomena.

4.2 Model Designing

Initially the device had been modeled with a single layer and then it has been layered with the skin, bone, blood and fat. The circular finger at the bottom is the acoustic source that is on for a second and then it is shut off. The rectangular layers are filled with the skin and bone respectively. The elliptical layer serves as fat and the rest is filled in with the blood. Figure 4.1 shows the geometry of the single and multiple layers.

The properties of the materials that are used in designing the model are shown in table 4.1.

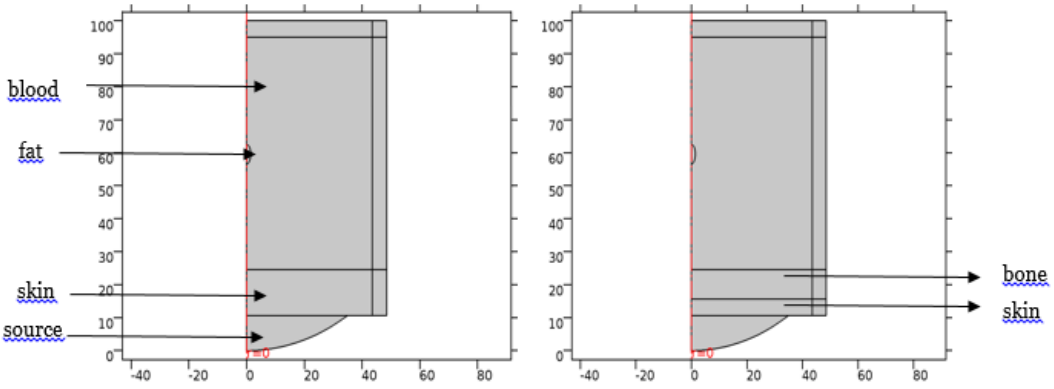

Fig. 4.1. Geometry showing single layer and multiple layers

Table 4.1.
Properties used of the materials used

Parameter	Value
Density of blood	1050
Density of fat	911
Density of skin	1109
Density of bone	1178
Electrical conductivity of blood	1.23
Electrical conductivity of fat	$6.48e^{-}2$
Electrical conductivity of skin	$4.91e^{-}1$
Electrical conductivity of bone	$1.73e^{-}1$
Speed of sound in blood	1578
Speed of sound in fat	1140.2
Speed of sound in skin	1624
Speed of sound in bone	2117.5
Heat capacity of blood	3617
Heat capacity of fat	2348
Heat capacity of skin	3391
Heat capacity of bone	1313
Temperature	293.7 K
Frequency	1Mhz,2Mhz,3Mhz

The figures 4.2 shows the elliptical layer filled with the properties of fat and the other layers filled with blood. The figure 4.3 shows the layer that is filled with the properties of the bone.

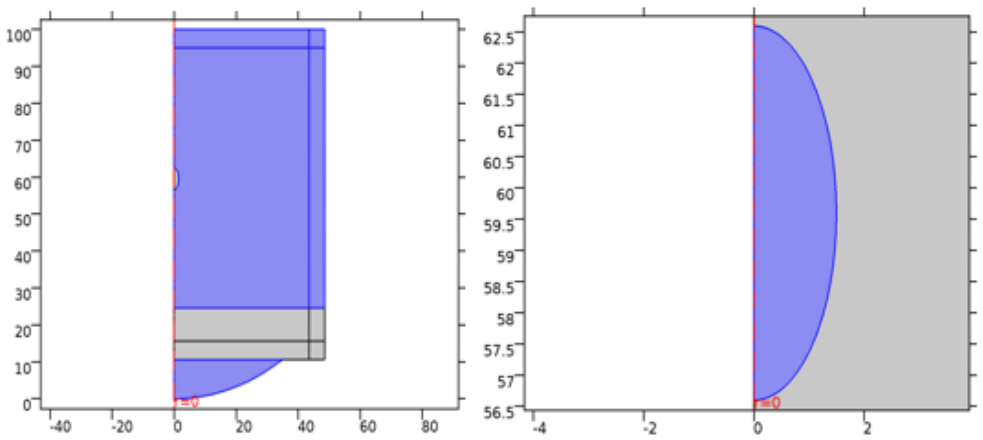

Fig. 4.2. Geometry showing single layer and multiple layers

The bottom layer of the device is filled with the skin.

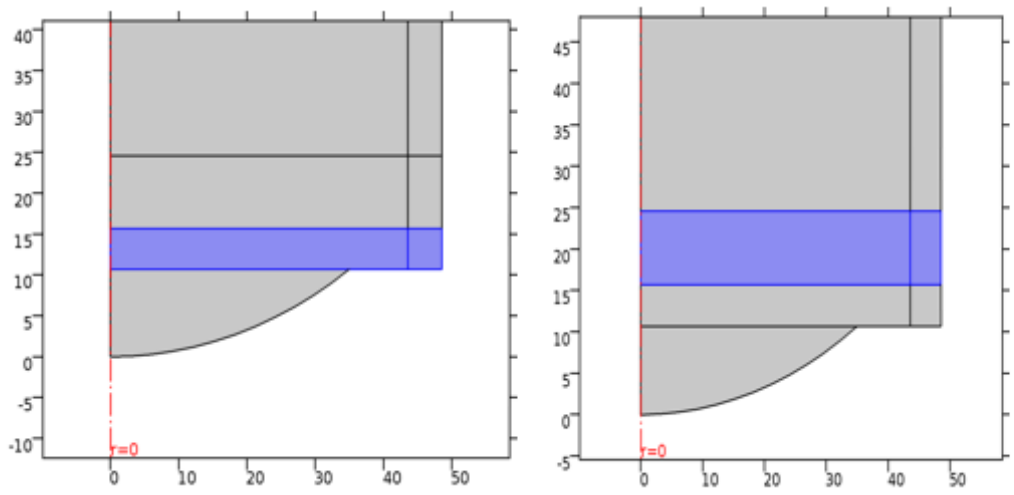

Fig. 4.3. Layers filled with the properties of bone and skin

Two different physics have been chosen for this model. The pressure acoustics module interfaced with the acoustics model from comsol has been chosen to fill in the entire model with the source shooting the acoustic waves into the fat. The given figure 4.4 represents the model interfaced with pressure acoustic physics.

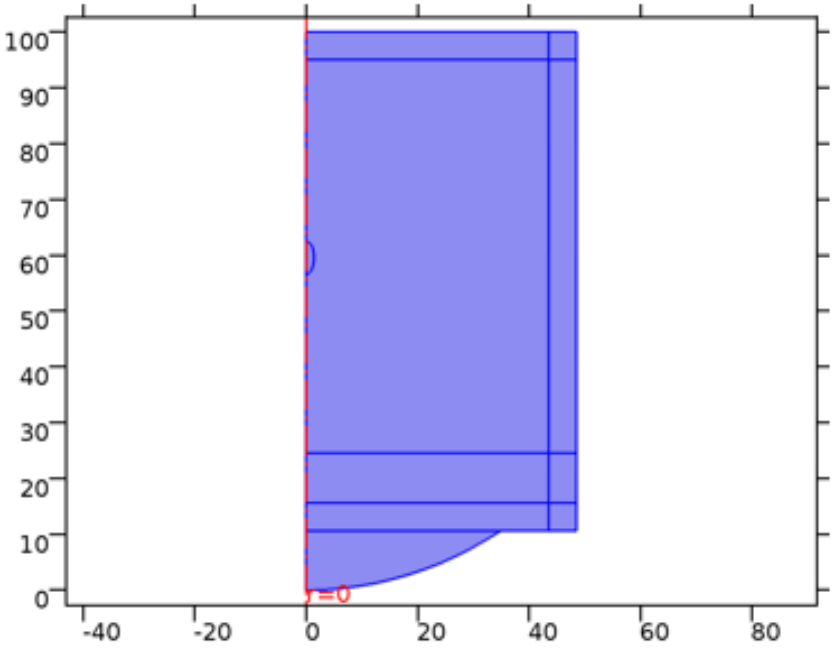

Fig. 4.4. Layers interfaced with pressure acoustics

The model requires the heat to be spread evenly inside the tissues after absorbing the acoustic waves. For this purpose the bio heat module form the heat transfer model is utilized. The bio heat physics inside the model is as shown in figure 4.5.

The model for this study assumes that the source is located at its bottom having

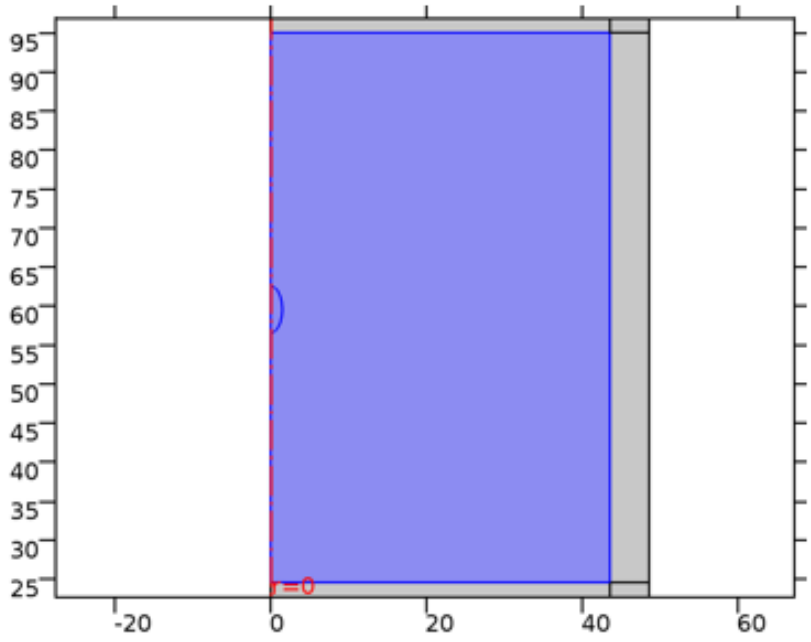

Fig. 4.5. Layers interfaced with bio heat

its complete focus merging into the fat. Therefore, the energy thermal and acoustic are focused at the artery site, propagating via the blood, bone, and skin. Figure 4.6 shows the layer set up for the simulation model. Figure 4.7 shows the mesh distribution with 12mm and 6mm meshes within 40 cm2 blood area. The system uses two types of meshes. A finer mesh for the corners near the fat region where the source energy is, and little thicker mesh for the blood region. The thinner mesh was chosen in order to cover the small size fat where the energy was localized.

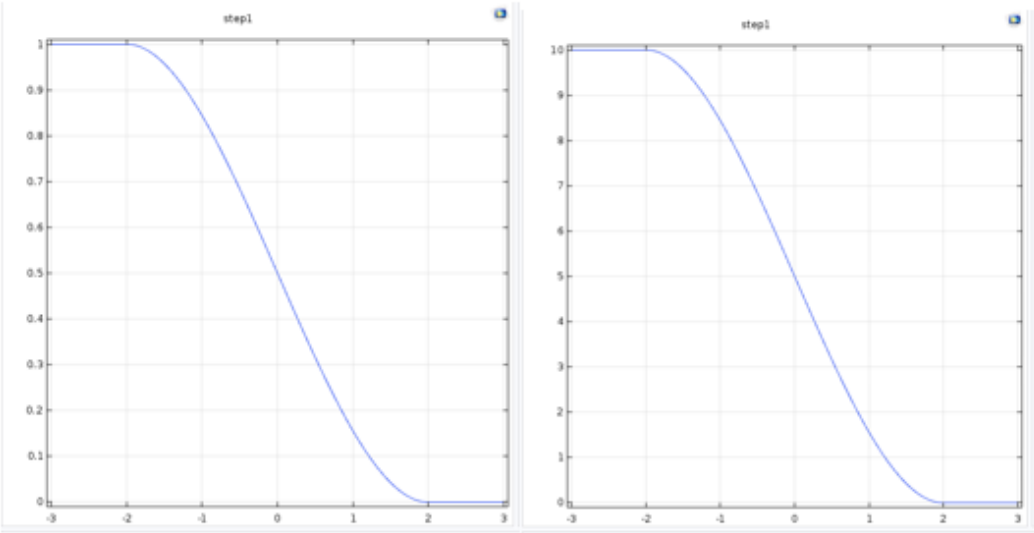

Fig. 4.6. Mesh distribution within the blood material, fat, skin and bone

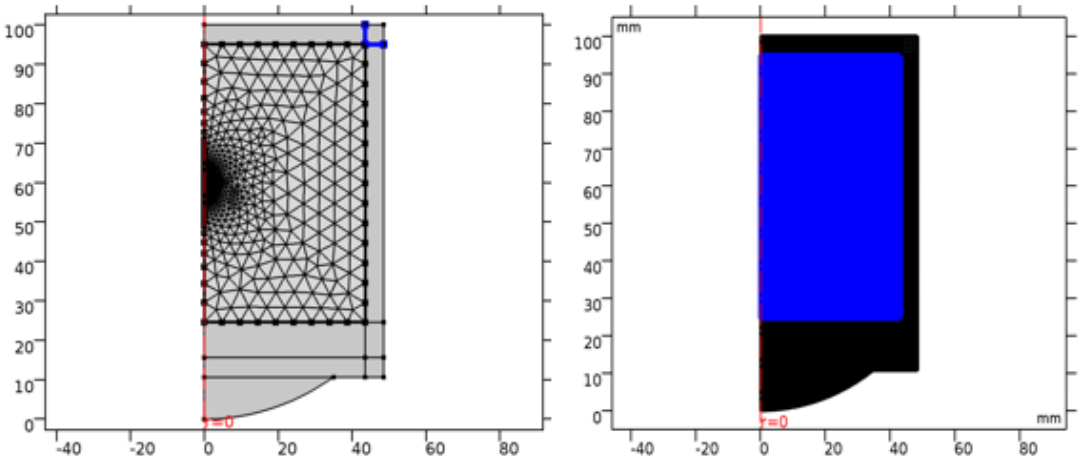

Fig. 4.7. Pressure pulse assumed for simulation

4.3 The Mathematical Models

Under the assumption that the source of energy was initially acoustic pressure, the energy conversion to bioheat occurs inside the various tissue layers. Therefore,

the solutions of dynamic acoustic pressure and temperature throughout the multiple tissue layers are governed by the two differential equations: the acoustic wave equation and the bioheat equation.

4.3.1 The Acoustic Wave Equations

An initial pressure of 1MPa was applied to the skin layer was applied. Figure 2 shows the pressure pulse assumed in the simulation. The acoustic wave equations used in this simulations are given as

$$\Delta.(\frac{-1}{\rho_c})(\Delta p_t - q_d))\text{-}\frac{(k^2{}_{eq}p_t)}{\rho_c}) = Q_{\mathrm{m}} \tag{4.1}$$

Where $p_t = p + p_b$, and p is the acoustic pressure and Pb is the biological thermal pressure.

$$K^2{}_{\mathrm{eq}} = (\frac{\omega}{c_{\mathrm{c}}})^2 - k^2{}_{\mathrm{m}}, k_{\mathrm{m}} = \frac{m}{r}c_{\mathrm{c}} = \frac{\omega}{k}, k = \frac{\omega}{c} - i\alpha, \rho_{\mathrm{c}} = \frac{\rho c^2}{c^2{}_{\mathrm{c}}} \tag{4.2}$$

Where m is the mass density, r is the location in space, ω is the radian frequency, Qm is the metabolic heat source, alpha is the absorption co-efficient and c is the speed of the sound. The boundary conditions by the normal components of the amplitude of the acoustic pressure wave at the boundary wall (see equation 4.3), and at normal displacement d_n (equation 4.4) are given by

$$\text{-}n.(\frac{-1}{\rho_c})(\Delta p_t - q_d)) = 0 \tag{4.3}$$

$$\text{-}n.(\frac{-1}{\rho_c})(\Delta p_t - q_d)) = (i\omega)^2 d_{\mathrm{n}} \tag{4.4}$$

Where n is the unit normal vector normal to the interface boundary, and is the material density.

4.4 Bio Heat Equations

$$\rho c_{\mathrm{p}} \Delta T + \Delta . q = Q + Q_{\mathrm{bio}} \tag{4.5}$$

$$Q_{\mathrm{bio}} = \rho_{\mathrm{b}} c_{\mathrm{p,b}} \Omega_{\mathrm{t_b\text{-}T}} + Q_{\mathrm{met}} \tag{4.6}$$

Where T is the temperature, is the density, Cp is the specific heat, k is the thermal conductivity, b is the density of blood, Cb is the specific heat of blood, wb is the blood perfusion rate, Tb is the temperature of the blood, Q is the heat, and Qmet is the metabolic heat source.

The model has been simulated for three different frequencies 1MHz, 2MHz and 3MHz.Frequencies greater than 3Mhz were also considered, but the software crashes for frequencies beyond 3Mhz. Apart from the point of focus two different out focus points have been considered and the change in temperature rise has been estimated.

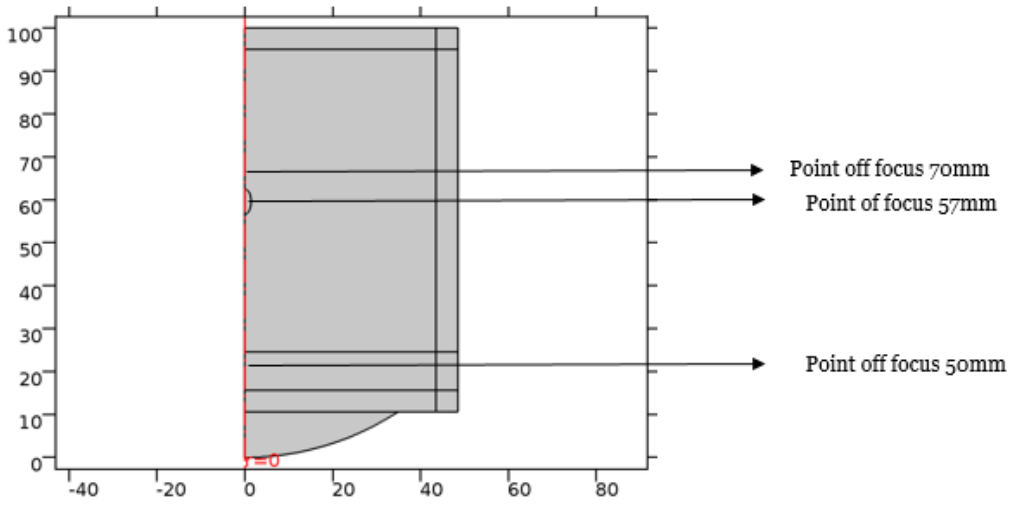

Fig. 4.8. Model showing different point of focuses

The acoustic pressure energy sourced at the fat region will result in thermal energy conversion that propagate into the fat, blood, and the skin regions. Furthermore, the reflected acoustic wave will also propagate via the same media. The thermal and acoustic propagation patterns may be analyzed for the distinction of the types of fat assumed in the simulation.

In the study, as indicated by the governing equations 4.7, 4.8, 4.9, the acoustic pressure is function of the frequency and magnitude of the acoustic pressure. In our simulation, we considered three types of energy as altered by the frequency 1mhz, 2mhz, and 3mhz.The p_0 source was also altered to increase the energy level.

$$I = \frac{1}{2}\rho v(\omega)^2 x^2 \tag{4.7}$$

$$I = PV \tag{4.8}$$

Comparing 4.7 and 4.8 we get a relation between the angular frequency and the pressure.

$$p \propto \omega^2 \tag{4.9}$$

5. RESULTS AND DISCUSSIONS

5.1 Introduction

In this work, COMSOL simulation was utilized in order to estimate the acoustic pressure and thermal distribution for individual and multiple layers. Skin, blood, fat, bones are the individual tissues considered in the study. The simulation addresses the effect of tissue thicknesses, frequency, pulse energy, and penetration depths throughout the individual layers.

5.2 Energy Conversion within the Multilayer Structure

The initial energy transmitted into the multiple layers was acoustic pressure in Pascal (N/m^2), which is measure in $Joule/m^3$. This energy was transmitted and partially converted to thermal energy. The latter may be determined via the thermal parameters in relative to the acoustic parameters of the various layers. For instance, the acoustic energy is determined from the acoustic impedance, frequency and Grneisen parameter while the thermal energy is determined by the specific heat capacity and thermal conductivity. The ratio of the two output energies (thermal and acoustic) were determined by COMSOL software. It appears that the thermal energy changes via the different layers and propagate following the heat equation described in chapter 4. The response of both output energies were determined from the combined solution of the acoustic and heat equations. The boundary conditions were set to determined. both T and P at the different interfaces. The following equations clarify the process:

W_0 (the initial energy)= $W_1(acousticenergy) + W_2$ (the thermal energy)

The expression for acoustic energy has been explained in chapter 4, the ratio between W_1 and W_2 are determined based on the parameters pressure and intensity. These are material based parameters and change from one layer to another.

5.3 Research Parameters

After designing the model, frequency domain analysis and time dependent analysis is done. The analysis are done using the pressure acoustics followed by Bioheat model approach help us obtain the acoustic pressure intensity and thermal distribution. The analysis is done on multiple layers starting with a single layer of bone followed by

1) Bone and skin
2) Bone, skin and fat
3) Bone, skin, fat and blood

The change in temperature and sound pressure for different energy levels and different thickness is noted.

5.3.1 Study 1: Acoustic Pressure Versus Frequency Domain

Initially the study is computed for pressure acoustics at different frequencies with physics defined for pressure acoustics keeping the bioheat unselected. A finer mesh is used for the analysis of study 1. This study is further used for generating data sets such as revolution 2D, mirror 2D. These data sets help us in obtaining the graphic solutions such as acoustic pressure, sound pressure and also various temperature distributions but varying the frequency.

5.3.2 Study 2: Transient Analysis, Time Domain

Next the study is solved for the bioheat model in time domain using the transient analysis. This study uses a mesh that is finer than the mesh used in the study 1. The study 2 is used to produce data sets such as cutline 2D and cut point 2D. These data sets help us in producing various plots such as acoustic pressure field, temperature profile with various rise times and fall times.

5.4 Data Sets

Solutions correspond to data stored by the solvers. Every solver is linked to a data set. Data sets help us in generating the data that is needed to create the expected visual results.These help us in evaluating and organizing the results. Data sets are analogous to the data that is stored in the solvers. Every solved model in comsol is expected to have a data set. Data sets do not change the expected output. For the simulation of this research work data sets such as revolution 2D, cut point 2D, cut plane 2D and mirror are created.

5.4.1 Revolution 2D

The current simulation has two sets of revolution 2D data sets in it. Revolution 2D is used for generating the 3D structures using the 2D axial geometry and it helps us in knowing what happens in the 3D. Two sets of revolution 2D (revolution 2D 1 and revolution 2D 2) are generated for 3D temperature and sound pressure level. Figure 5.1 represents the revolution 2D 1 and revolution 2D 2 used for the simulation

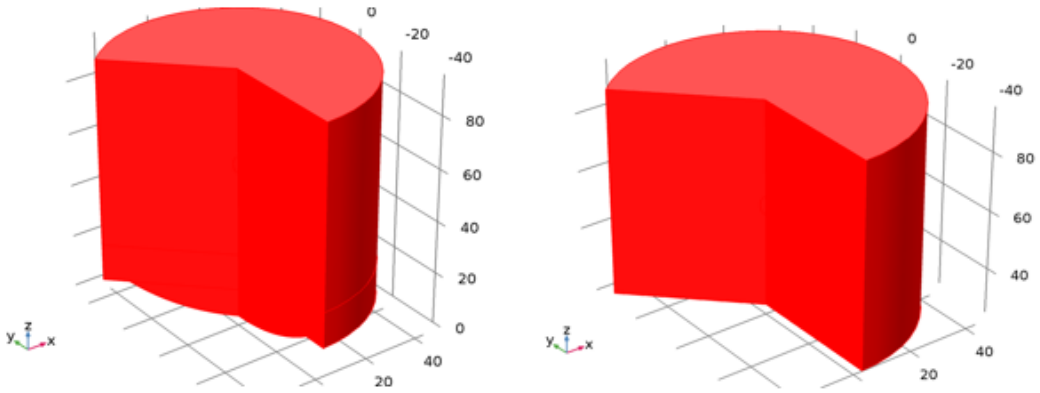

Fig. 5.1. Revolution 2D1 and Revolution 2D 2

5.4.2 Mirror 2D

Mirror data sets are used for better visualization of the outputs. Two sets of mirror 2D data sets are generated one for the better visualization of the acoustic pressure and the other for the better visualization of the temperature field. Figure 5.2 represents the mirror 2D 1 and mirror 2D 2 used for the simulation

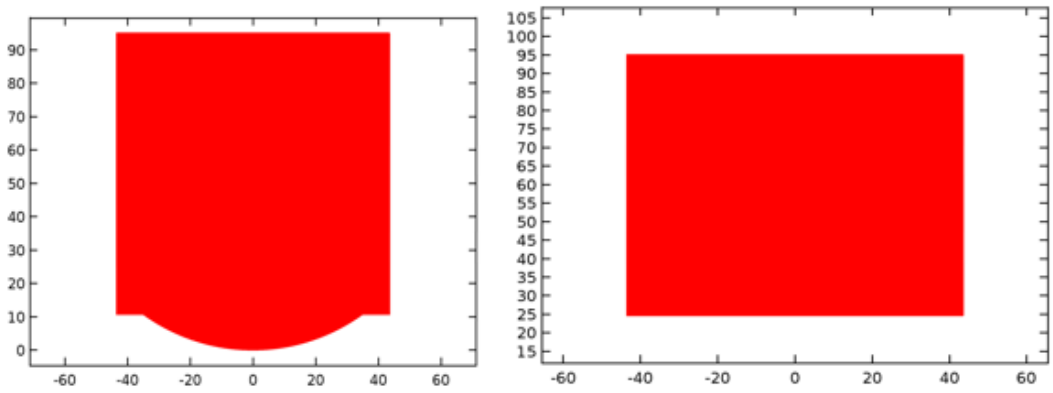

Fig. 5.2. Mirror 2D1 and Mirror 2D 2

5.4.3 1D Plot Group

1D plots are generally used plot line graphs are needed and these are little different from using 2D and 3D.

5.4.4 Cutline 2D

Cutlines are generally used to evaluate the variables and see the results along a line. Cutline 2D is used to generate the plot for acoustic pressure amplitude along the radial direction in focal plane for 1sec and 2sec. Figure 5.3 represents the cutline 2D 1 and cutline 2D 2.

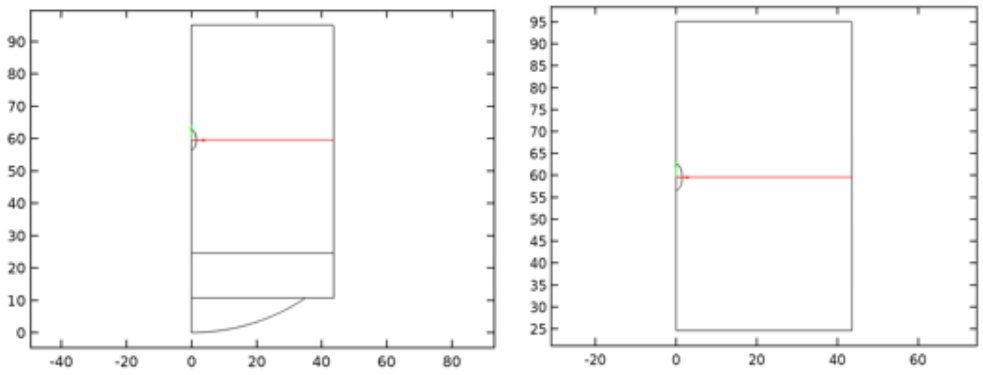

Fig. 5.3. Cutline 2D1 and cutline 2D 2

5.4.5 Cut point 2D

Cut point 2D data sets are used to evaluate the variables at specific point as shown in figure 5.4. It can be placed anywhere in the geometry and it does not affect the output. In this simulation cut point 2D is used for plotting the temperature rise and fall curves at acoustic focus and 0.5mm off the focus. Cut point 2D 1 and cut point 2D 2 are given in Figure 5.4.

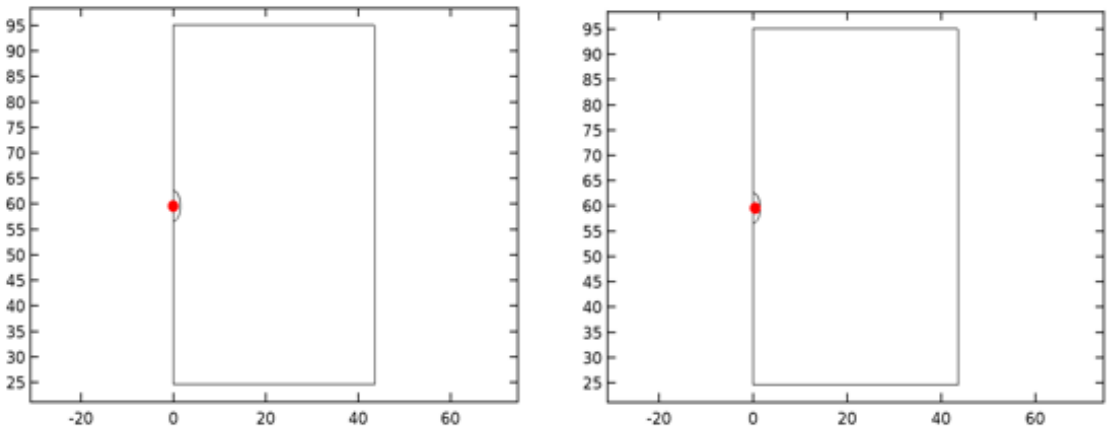

Fig. 5.4. Cutpoint 2D1 and cutpoint 2D 2

5.5 Bone Tissue Simulation

The acoustic pressure field is observed to be high at the focal point and it is decreasing as it goes out of the focus point. The total acoustic pressure field indicates the presence of the fat inside the arteries differentiating the pattern in between the fat at the focal point and the skin that is located as a layer at the bottom. Figure 5.5 shows the total acoustic pressure. When the figure 5.5 is observed, it can be seen that the fat tissue has observed most of the acoustic pressure while the other layers have absorbed very little acoustic energy.

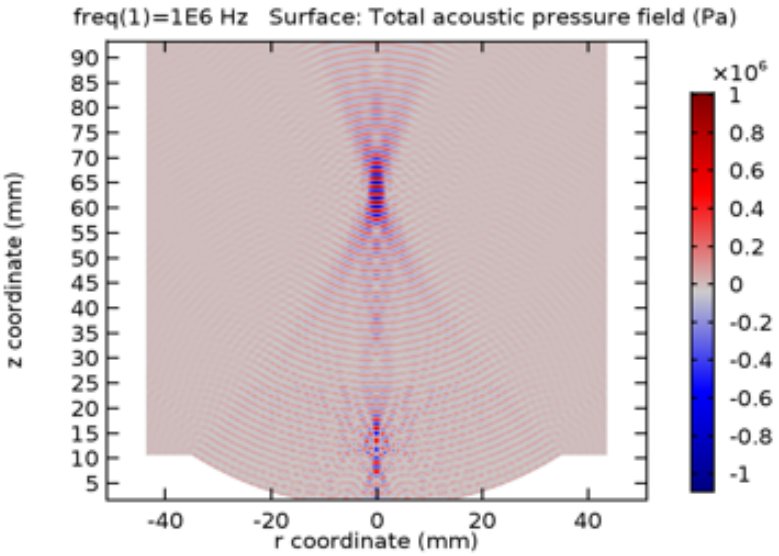

Fig. 5.5. Total acoustic pressure field

5.5.1 1 MHz/ One Joule Energy Simulation

5.4.1.1 Fat tissue

In this case, the energy source is applied to LDL fat source, and the simulation was determined at three difference locations to data analysis. The simulations were determined at 50mm (9.6 mm below the fat center area), 57mm (1.5 mm from the center fat area), and 70mm (10.4mm above the fat center region) are as follows. The temperature at the point of focus remains constant but the temperature drops as we go out of focus.

At focus, the temperature absorbed was 3.4° K above the body temperature (293.9° K), while off focus the temperature at 57mm was estimated to be 2° K, and was dropped to 0.4° K, and 0.45° K at 50mm and 70mm respectively. A temperature change of ΔT=3.4 - 2 = 1.4° K occurred at 57mm, a change ofΔT = 3.4 - 0.4 = 3° K at 50mm, and a change of ΔT = 3.4 - 0.45 = 2.95° K at 70mm. It is clear that the temperate dropped to 0.5° K near the bone area. Figure 5.6 shows the temperature profile for the fat material at 50mm, 57mm, and 70mm at 1MHz.

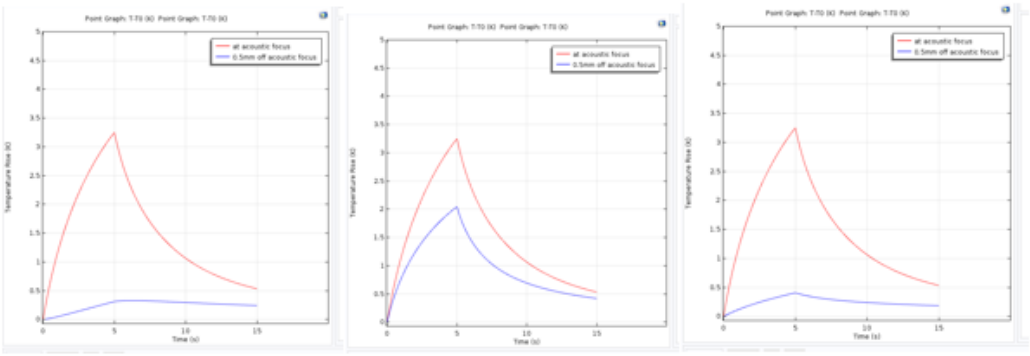

Fig. 5.6. Temperature profile for fat at 50mm, 57mm, 70mm at 1MHz

5.4.1.2 Nonfat tissue

Similar simulation was done considering a non-fat material source, and the temperature distribution was determined at the three locations 50mm, 57mm and 70mm for 1 MHz. Figure 5.7 shows the temperature profile for non-fat material at 50mm, 57mm, and 70mm at 1MHz.

The temperature at focus dropped when material used is nonfat. The temperature at focus was 2° K while it is 0.9° K at 57mm, 0.4° K at 70mm and it is almost zero at 50mm. At focus the temperature was 2° K, while off focus the temperature at 57mm is 1° K, and was dropped to 0.3° K and 0.4° K at 50mm and 70mm. A temperature

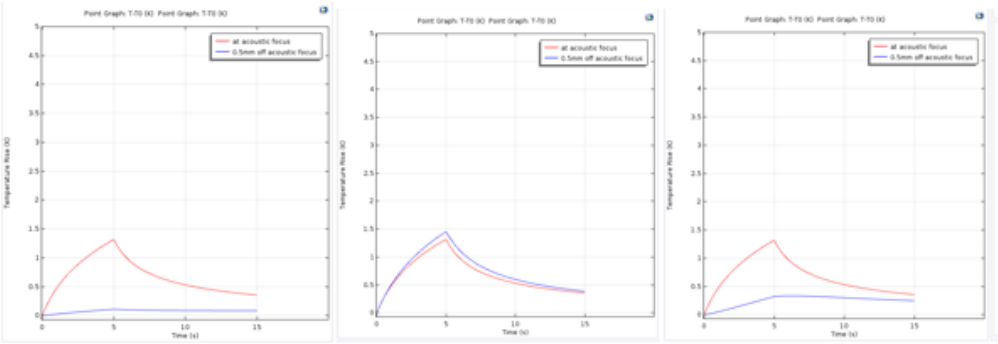

Fig. 5.7. Temperature profile for nonfat at 50mm, 57mm, 70mm at 1MHz

change of $\Delta T = 1.4 - 1.3 = 0.1^\circ$ K occurred at 57mm, and a change of $\Delta T = 1.4 - 0.25 = 1.15^\circ$ K at 50mm, and a change of $\Delta T = 1.4 - 0.4 = 1^\circ$ K at 70mm.

5.5.2 2 MHz/ One Joule Energy Simulation

With the increase in frequency the temperature increases. The temperature at the point of focus rises to 27° K. While the temperature off focus is less at 50 mm and 70 mm compared to the temperature at 57mm. The temperature for the nonfat decreases when compared to the temperature for fat. A temperature change of $\Delta T = 23 - 12 = 11^\circ$ K has been observed at 57mm while a change in ΔT of $\Delta T = 23 - 0 = 23^\circ$ K at 50mm and 22° K 70mm has been noticed. Figure 5.8 shows the temperature profile for fat material at 50mm, 57mm, and 70mm at 2MHz frequency.

For non-fat material the temperature at focus decreases to 9° K at focus while a change in temperature $\Delta T = 9 - 7 = 2^\circ$ K has been noticed at 57mm while the change remains 9° K at 50mm and 8° K 70mm. Figure 5.9 shows the temperature profile for nonfat material at 50mm, 57mm, and 70mm at 2MHz frequency.

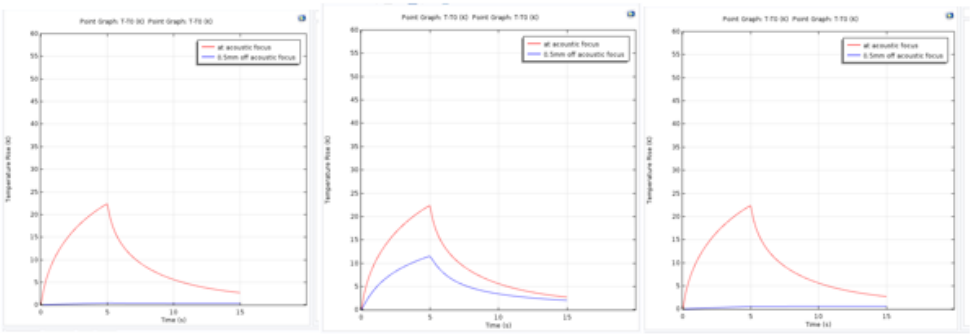

Fig. 5.8. Temperature profile for fat at 50mm, 57mm, 70mm at 2MHz

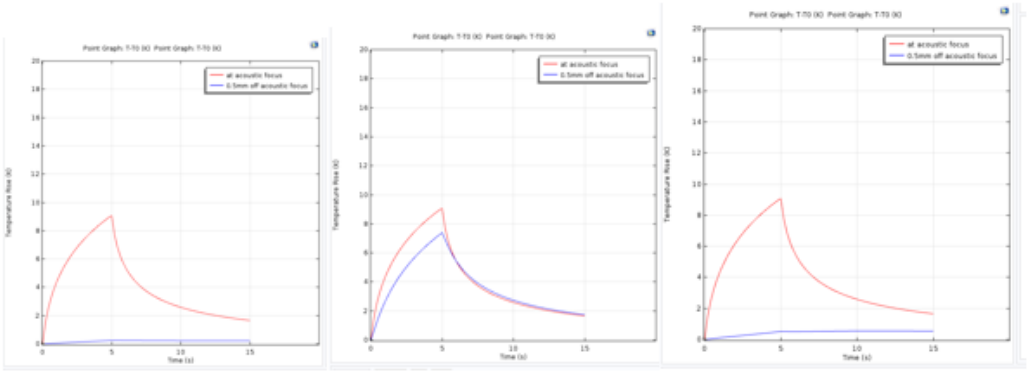

Fig. 5.9. Temperature profile for nonfat at 50mm, 57mm, 70mm at 2MHz

5.5.3 3 MHz/ One Joule Energy Simulation

The simulation given here is based on the same energy but the frequency is increased to 3MHz. The temperature at the point of focus increases to 43° K at the point of focus while a change in temperature of ΔT =43 - 25 = 18° K has been observed at 57mm, and a change remains 43° K at 50mm and 42° K at 70mm.

Figures 5.10 and 5.11 give the temperature profile for the fat and non-fat materials respectively at 50mm, 57mm and 70mm.

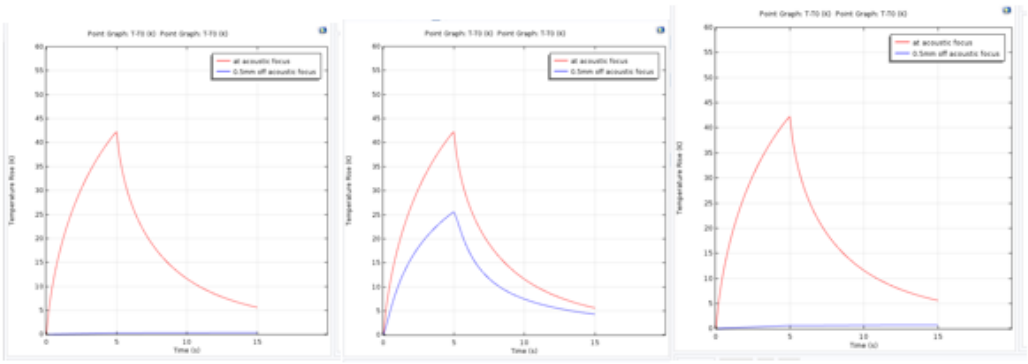

Fig. 5.10. Temperature profile for fat at 50mm, 57mm, 70mm at 3MHz

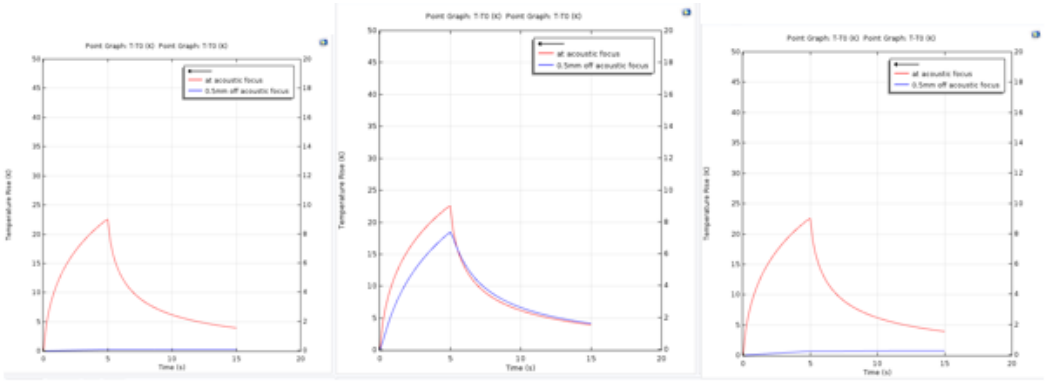

Fig. 5.11. Temperature profile for nonfat at 50mm, 57mm, 70mm at 3MHz

In a similar pattern, the temperature at focus drops to 23° K for nonfat material. We also noticed a temperature change of $\Delta T = 23 - 18 = 5°$ K at 57mm and the change in temperature ΔT remains 23° K at 50mm and 22° K at 70mm. Figures 5.12 gives the distributions at the bone materials for 1MPa.

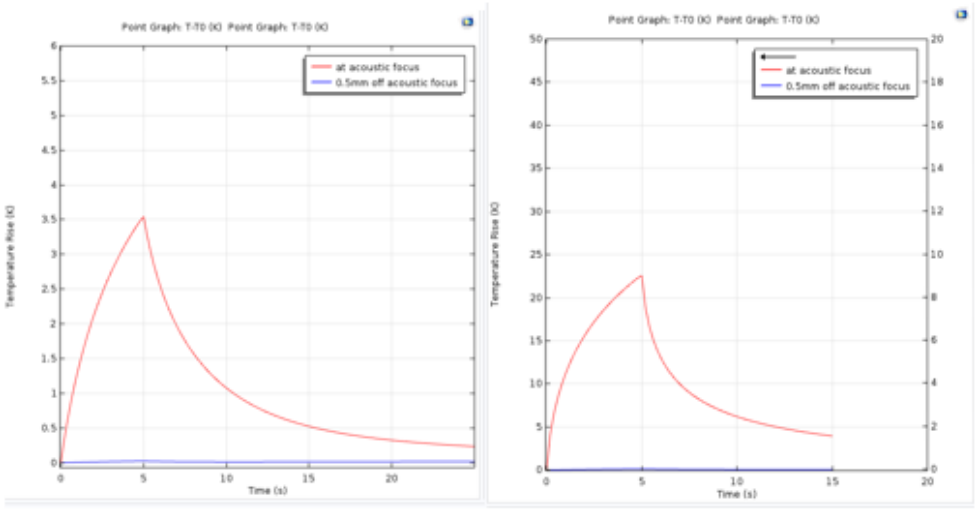

Fig. 5.12. Temperature distributions at the bone materials for 1MPa

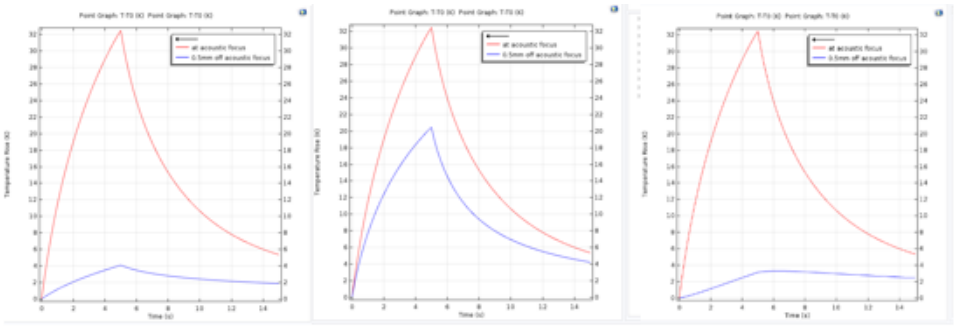

Fig. 5.13. Temperature profile for fat at 50mm, 57mm, 70 mm at P_0 =10MPa at 1MHz

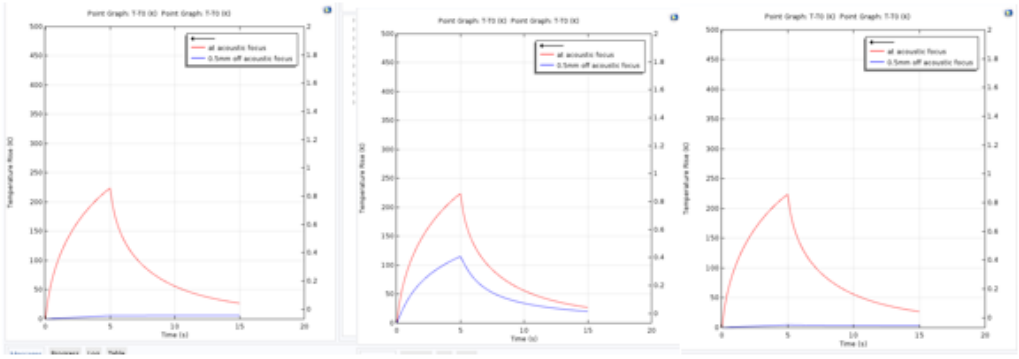

Fig. 5.14. Temperature profile for fat at 50mm, 57mm, 70 mm at P_0 =10MPa at 2MHz

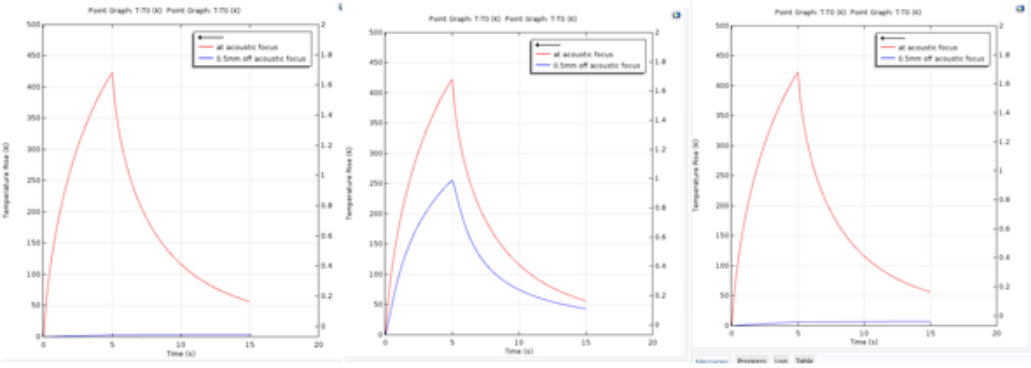

Fig. 5.15. Temperature profile for fat at 50mm, 57mm, 70 mm at P_0 =10MPa at 3MHz

The temperature near the bones is zero hence an increase in the pressure pulse have been made to notice a significant temperature change at the bones. The simulations for P_0 = 10MPa at 50mm, 57mm and 70mm for the frequencies 1MHz, 2MHz and 3MHz are shown respectively in Figures 5.13, 5.14 and 5.15. The simulations at bones for when the pressure pulse has been raised to 10 in Figure 5.16.

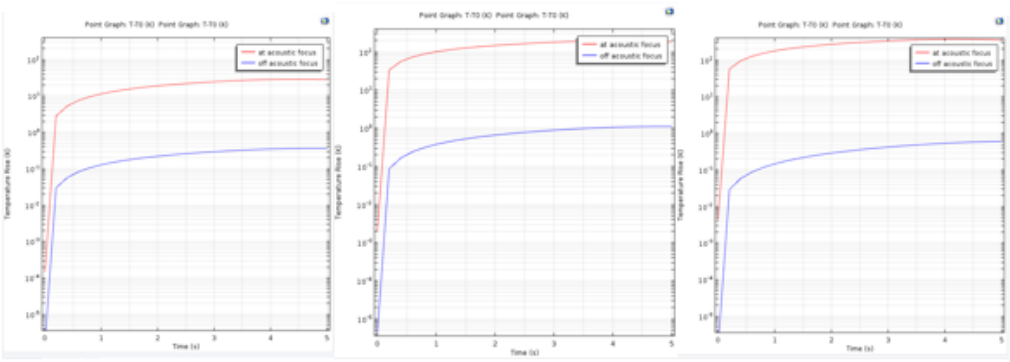

Fig. 5.16. Temperature profile for bones at P_0 =10MPa for1MHz, 2MHz and 3MHz

5.6 Acoustic Pressure Profile

Sound pressure has been investigated for 1MHz, 2MHz and 3MHz. The output has been observed to be higher from 240dB to 260 dB as we increased the frequency at the point of focus. Figure 5.17 represents the pressure that is being used at the point of focus and the total acoustic pressure that is being lost. The point of focus is at 59.6mm and the energy that is being reflected beyond the 59.6mm point is lost.

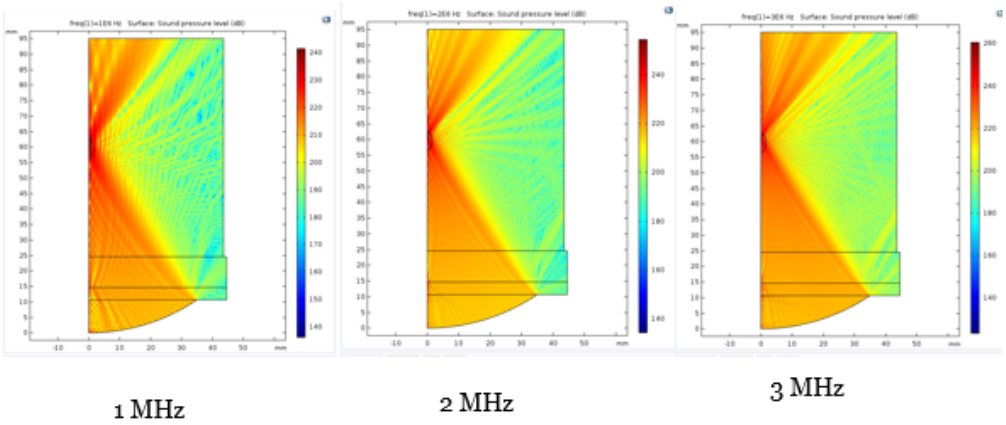

Fig. 5.17. Pressure at the point of focus and the total acoustic pressure that is lost

Figure 5.18 and Figure 5.19 represent the total acoustic pressure plotted to the pressure amplitude. These plots helps us in noticing the significant power that is being dissipated beyond the point of focus. With the increase in frequency the amount of energy dissipated as loss also increases with the increase in acoustic pressure.

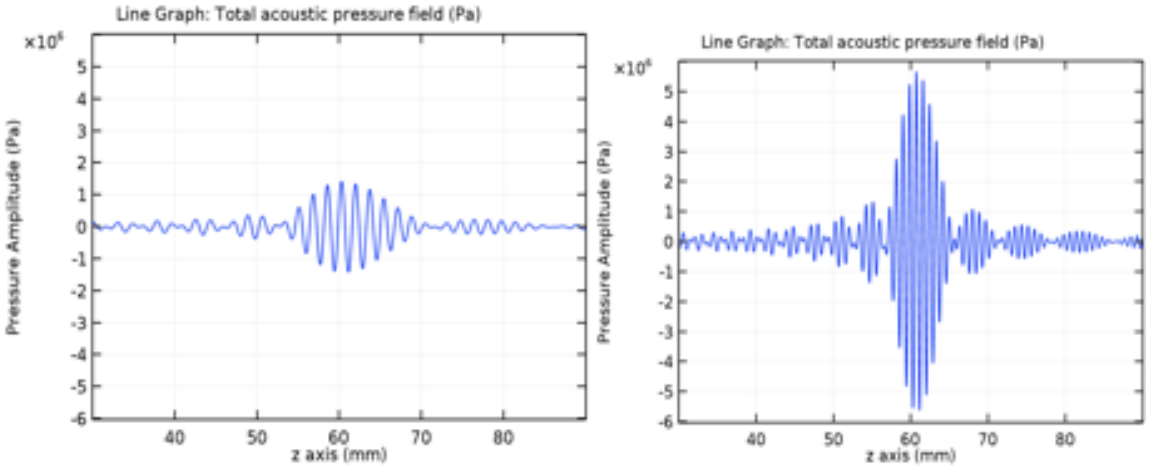

Fig. 5.18. Acoustic pressure field for 1MHz and 2MHz

Figure 5.20 shows a comparison between the variation in acoustic pressure fields for a single layer tissue and multilayer tissue at 1MHz.

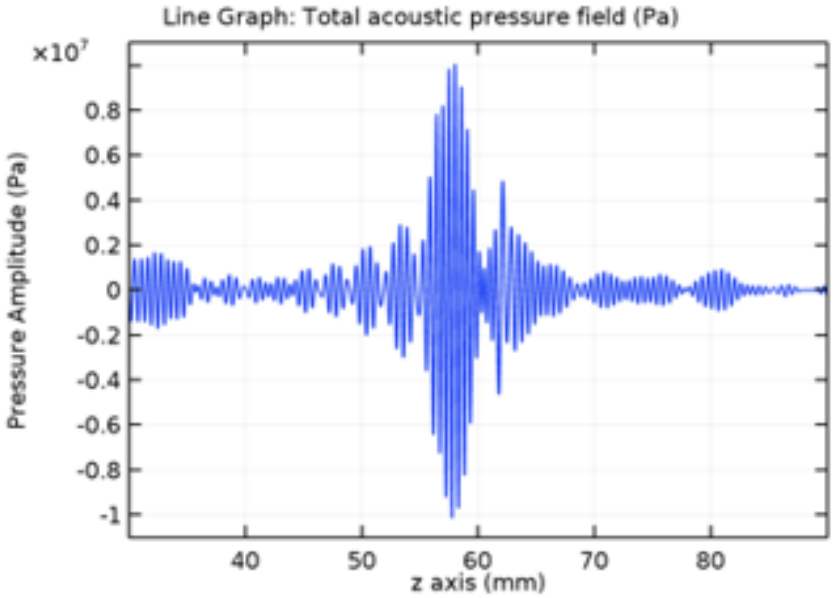

Fig. 5.19. Acoustic pressure at 3MHz

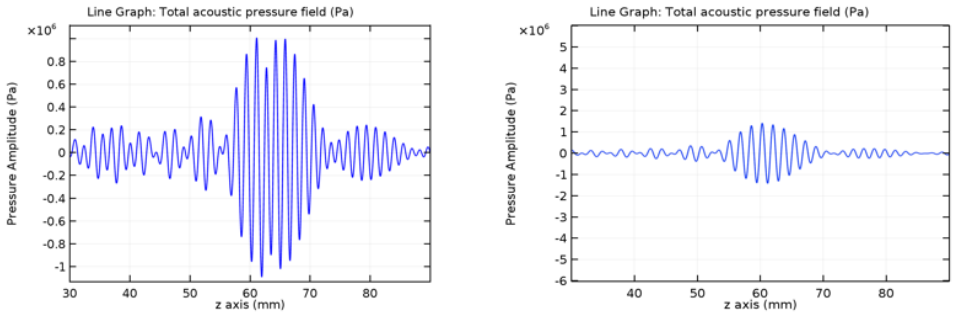

Fig. 5.20. Acoustic pressure for single layer and multilayer tissue at 1MHz

5.7 Impact of the thicknesses

The study has been extended to include the impact of the thicknesses on the power transmission (thermal and acoustic). In that study, we considered two different

thicknesses for the bone tissue materials. The impact may be attributed to the different acoustic impedance of the tissue materials at given thicknesses, and the power transmission and reflections of the overall multilayer structure. This issue is important for the variations of the tissue thicknesses for different patient's conditions. The above data was investigated for 5mm bone thickness. The following simulation gives the impact when 10mm thickness was considered.

5.7.1 Under the Condition of P_0 =1MPa

With 1MHz

Thickness of skin and thickness of bone has been increased. With the change in thickness the temperature drop at the point of focus and off focus has been noticed. A $\Delta T = 4.8 - 1.2 = 3.6°$ K has been observed when the thickness of the bone has been increased. The temperature change with increase in skin was noticed to be slightly greater than the change observed with the increase in temperature. A $\Delta T = 4.9 - 1.2 = 3.7°$ K was noticed. Figure 5.21 and 5.22 show the temperature, acoustic pressure field, pressure when thickness of skin and bone are varied.

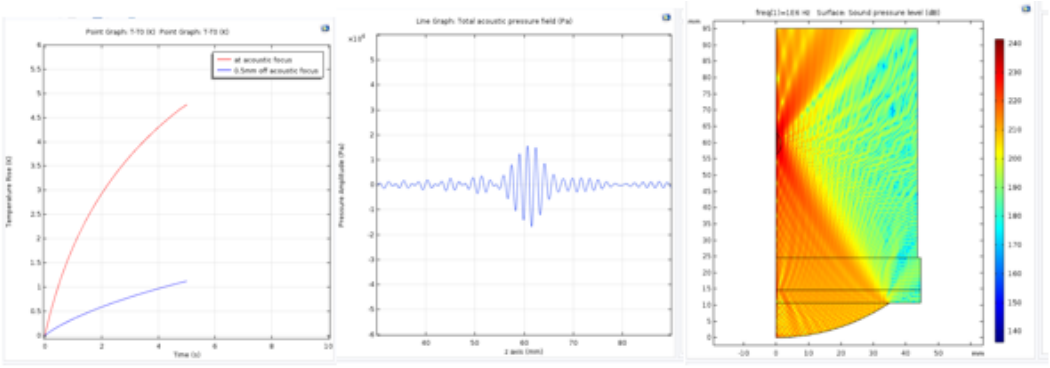

Fig. 5.21. Temperature, acoustic pressure field, pressure at 1MHz with thicker bone

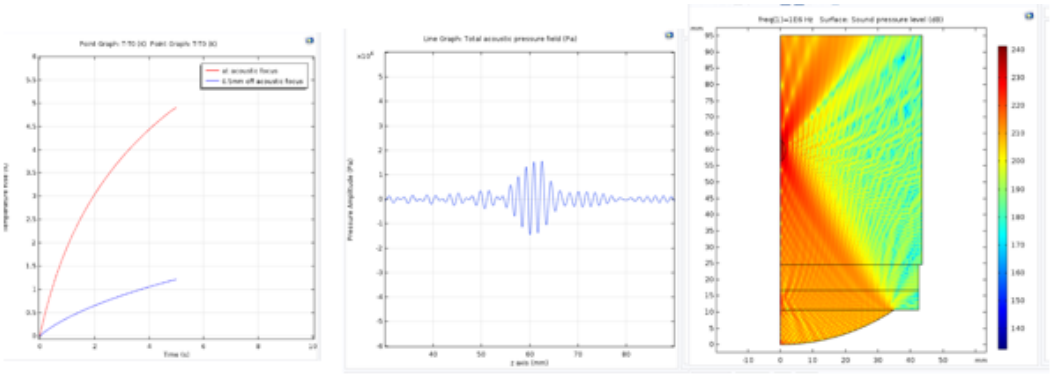

Fig. 5.22. Temperature, acoustic pressure field, pressure at 1MHz with thicker skin

With 2MHz

The frequency has been raised to 2MHz and the change in temperature has been noted by increasing the thickness of the skin and bone. When the thickness of the bone is greater than the thickness of the skin, a temperature change of $\Delta T = 14 - 8 = 6^{\circ}$ K has been noticed. Further the thickness of the skin has been increased and a temperature change of $\Delta T = 21 - 9 = 12^{\circ}$ K has been seen.

Figure 5.23 and 5.24 show the temperature, acoustic pressure field, pressure when thickness of skin and bone are varied at 10MPa for 2MHz frequency.

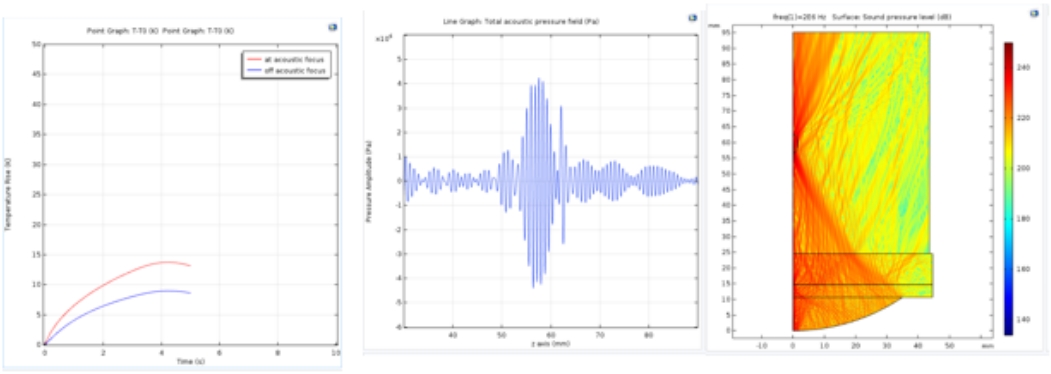

Fig. 5.23. Temperature, acoustic pressure field, pressure at 2MHz with thicker bone

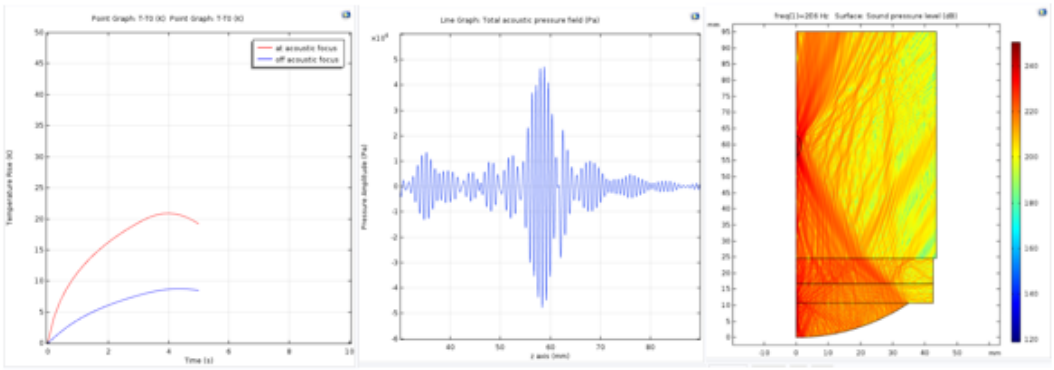

Fig. 5.24. Temperature, acoustic pressure field, pressure at 2MHz with thicker skin

5.7.2 Under the Condition of P_0 =10MPa

With 1MHz

Further the pressure has been increased to 10MPa to notice a significant rise in temperature near the bones. At 1MHz frequency a temperature change of ΔT = 50 - 10 = 40° K has been noticed and when the thickness of the skin is greater a temperature change was observed to be the same. Figure 5.25 and 5.26 show the

temperature, acoustic pressure field, pressure when thickness of skin and bone are varied at 10MPa for 1MHz frequency.

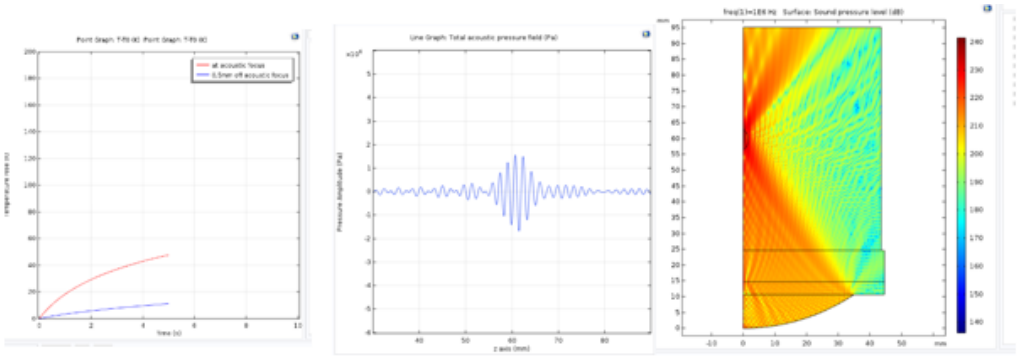

Fig. 5.25. Temperature, acoustic pressure field, pressure at 1MHz with thicker bone at P_0 =10MPa

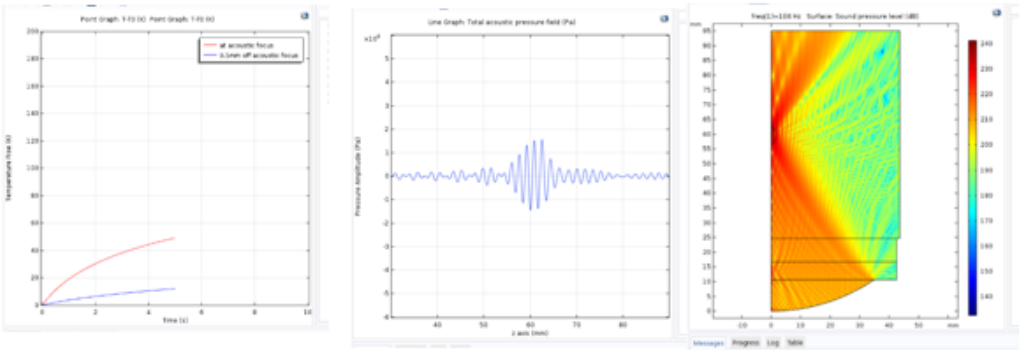

Fig. 5.26. Temperature, acoustic pressure field, pressure at 1MHz with thicker skin at P_0=10MPa

With 2MHz

The frequency has been raised to 2MHz and the change in temperature has been noted by increasing the thickness of the skin and bone. When the thickness of the bone is greater than the thickness of the skin, a temperature change of ΔT = 300 - 40 = 260° K has been noticed. Further the thickness of the skin has been increased and a temperature change of ΔT = 260 - 30 = 230° K has been seen. Figure 5.27 and 5.28 show the temperature, acoustic pressure field, pressure when thickness of skin and bone are varied at 10MPa for 2MHz frequency.

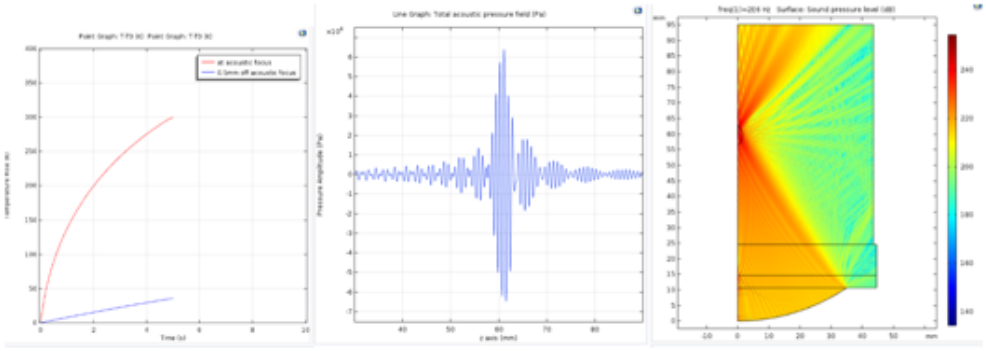

Fig. 5.27. Temperature, acoustic pressure field, pressure at 2MHz with thicker bone at P_0=10MPa

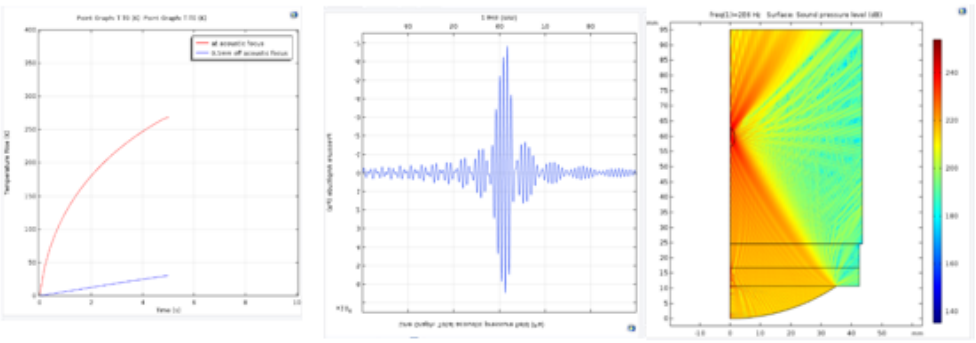

Fig. 5.28. Temperature, acoustic pressure field, pressure at 2MHz with thicker skin at P_0=10Mpa

5.8 Conclusion

The analysis of the photo acoustic approach for the diagnosis of type of fat inside human arteries showed promises for future implementation. It is suggested that the future approach focuses on the fat present inside the skin and the bones as well. The simulation considered different types of bones and skin with varying thicknesses.

The differences in pressure and temperature throughout the multiple tissue layers indicate the ability for MEMS and NEMS devices to detect the change.

In temperature and acoustic pressure parameters. The research parameters investigated in this work cover the frequency, tissue thickness, and acoustic pressure. The acoustic pressure and frequency were Parameters used for investigating the proper non-invasive approach covered in this work, while the tissue thicknesses are patient specifics.

Since the findings depend on the patient thicknesses, the approach followed here suggest that the impact of frequency and acoustic pressure for a given thickness should lead to a proper diagnostic approach.

The temperature change for all cases were ranging between 1.4° K, and 175° K, which is very doable via MEMS devices. Chapter 6 details future implementation for the typical temperature and acoustic pressure change as received from ten result section of this work.

There have been efforts done to run the simulation for higher frequencies such as 20MHZ as seen by other research efforts in the field, however, simulation at this high frequency showed some instability in the simulation. This may be attributed to software ability to run at this very high frequency for multiple tissue thicknesses. Even though, the three frequency values used in the study were sufficient and provided clear findings on the issues.

The temperature change and acoustic change given for different tissue thicknesses may be attributed to the change in the acoustic impedances of the different layers. The mismatching impedances of the different layers may lead to different power transmission.This was clearly covered in chapter 3 of the thesis.

The ratio between the acoustic and thermal energy generated from the initial acoustic energy may be estimated for the hardware design that could be more suited to the higher energy exhibiting the arterial information. This is reserved for future work.

5.9 Data Analysis

The following data summarize the impact of the acoustic energy as the frequency changes from 1 to 3MHz, and the effect of the acoustic power as P_0 changes from 1 to 10MPa. The temperature and acoustic pressure profiles while propagating and penetrating throughout the multiple layers are summarized below.

Table 5.1.
Data analyzed fro temperature, acoustic pressure field, and surface acoustic pressure

Parameters	**Pressure**						**Thicknesses**			
	1MPa			10MPa			4mm		6mm	
	1MHZ	**2MHZ**	**3MHZ**	**1MHZ**	**2MHZ**	**3MHZ**	**1MHZ**	**2MHZ**	**1MHZ**	**2MHZ**
ΔT	1.4	11	18	12	110	175	50	260	40	230
surface acoustic pressure	240	250	260	240	250	260	240	240	250	250
Acoustic pressure field	1.5	6	10	1.5	7	10	1.5	7	1.5	7

6. FUTURE WORK

6.1 Introduction

In this chapter we elaborate on the practical model of the system that enables monitoring the dynamic and special temperature and acoustic pressure distribution throughout the multiple layers from the human artery until beyond the skin layer. This hardware monitoring system will assist with the medical diagnosis for various patients. The research parameters obtained in the result section of the thesis have led to the proper selection of the hardware devices and processing units. Data received from the artery were both acoustic pressures and infrared. Therefore, the focus of this chapter is seeking IR sensors that can detect the ΔT(temperature) dynamic change throughout the human body, and the acoustic pressure sensors that can detect a change of nearly a small fraction of Mega Pascal. The devices proposed here are generally sensors that can detect a change in temperature within the body. The choice of these sensors was based on their ability to monitor the artery temperature and acoustic distribution from outside body.

6.2 Infrared Devices

High technology IR sensors are used in wireless communication between a transmitter and a receiver. In this case, however, the IR sensors are meant to be temperature detectors from a distance (to detect the temperature at the artery and throughout the body from outside).

Generally infrared devices can communicate from short distance to medium range distances within the centimeter range, depending on the mode of the device; near, mid and far waves. One of the best examples of an infrared device is the TV remote

controller. IR communication cannot be established between two rooms and IR rays cannot pass through the walls. Acoustic devices are generally used for amplification or to produce the sound waves. Most of the photo acoustic signals are generally used for imaging purposes. These devices are used for both invasive and noninvasive imaging. In invasive imaging the devices are manufactured as probes and sent into the human body. Infrared signals lie in between the visible light and micro wave signals i.e the region in between the 0.75 μm and 1000 μm in the electromagnetic spectrum is termed as the infrared region. According to Plancks radiation law, infrared rays are emitted by any object that has its temperature greater than 0 kelvin.

IR sensors are electronic devices that are used for the detection of heat or motion by emitting or detecting the infrared radiation. Infrared sensors are classified into two types: passive infrared sensors and active infrared sensors. The sensors which emit and also detect the emitted signals are termed as active infrared sensors while the sensors that only measure the infrared radiation than emitting the signals are called as passive infrared sensors (PIR sensors).

IR sensors generally need an IR source, a transmission medium, an optical system, a detector and a signal processor. The IR rays needs a medium to be transmitted. The optical system is used to converge the IR rays into the detection system. Detectors are of two types: thermal and quantum. Thermal detectors are independent on the wavelength and has a material detector in them, while the quantum detectors depend on the wavelength. The output obtained from the detectors need to be amplified as they are very small magnitude in nature. Hence signal processors are required.

IR sensors finds its applications as radiation thermometers which detect the temperature of the body by direct contact, flame monitors which detect and monitor the emitted light from the flames, moisture analyzers, IR imaging, remote sensing, etc., IR imaging is one of the primary applications of the IR sensors. Thermal IR detectors map the detected temperature distributions on to the image.

6.3 Acoustic Sensors

Acoustic sensors are electronic devices that are used to measure the level of sound pressure. When acoustic waves travel through certain materials, the acoustic waves influence the material properties that they travel through. Any changes to the properties of these materials changes the amplitude and velocity of the acoustic waves, which are then captured by the transducers and then characterized into the digital output. The changes in the properties can be figured out by measuring the frequency or phase characteristics [82] [83]. All the devices need a piezoelectric layer to generate these acoustic waves. Pressure from electricity is termed as piezoelectricity which is the production of electrical charges out of mechanical stress. These sensors generally use two inter digital transducers (IDTs); one that converts the incoming signal into mechanical signal while the other converts the mechanical signal to electrical signal. Both the transducers are electrodes that are interlocked in a comb like structure. The frequency of the wave scan be altered with the change in the distance between the electrodes [84]. Change in length, width and position of these IDTs varies the performance of the sensors. These sensors are generally used in telecommunications industry in order to detect the disturbances and prevent the unwanted change in the output. These sensors also detect the mechanical failures in the components [85]. The infra-red modes are shown in Figure 6.1, where the near wave can detect a distance of 14000-4000 cm^{-1}, the mid will characterize materials within 4000-400 cm^{-1}, and the far can detect a distance in the order of 400-10 cm^{-1}. These distance ranges vary from one sensor to another. As it can be seen, a distance of near 10 cm^{-1} can be detected via IR devices.

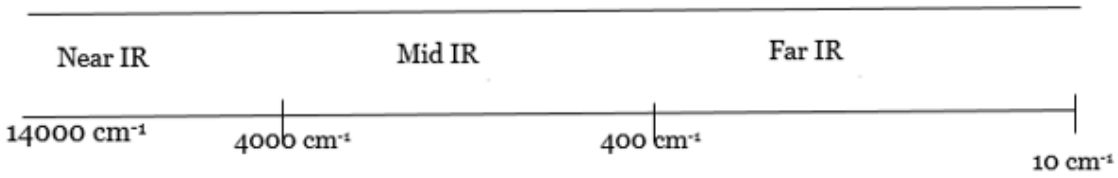

Fig. 6.1. IR modes

6.3.1 Approaches

Diagnostic approach is based on two main assumptions:
1) The initial energy is transmitted to the artery, and released from the artery into the body. The natural response of the energy through the bone, blood, and skin can be used in the medical diagnoses.
2) The initial energy is transmitted from outside until reached the artery, then the source of energy is then turned off, and let the energy at the artery released throughout the skin, fat, bone, and blood). Under this procedure, the assumption made was that the bone and skin materials have shorter fall time than the human artery. In this case, the energy in the artery is till stored, while the other materials have negligibly small energy.

6.3.2 The Focal Energy at the Artery

The transducers that can provide the first approach are devices that can shoot energy into the artery. These are preferred to have piezoelectric layer on top of the SiO2. Piezoelectric sensors, and are generally used to measure the change in pressure, strain, acceleration, temperature or force, by converting them into electric charge. Piezoelectric materials provide a high transformation of acoustical energy to bandwidth energy and vice versa [86]. They also provide high and uniform acoustical interaction with the semi conducting material [86]. ZnO and AlN are two popular ceramic piezoelectric materials considered in general. But ZnO has stronger piezoelectric coupling when compared to AlN [86]. On top of piezoelectric layer a layer of gold is assumed to be deposited because it has high electrical conductivity, providing better resistance to oxidation, low hardness and reduction to the signal attenuation [87].

The fabrication of the device take place in four steps. The first step involves the removal of the oxide layer from the substrate. Reactive ion etching process can be used for the removal of the oxide layer. Now a layer of ZnO is sputtered onto the wafer.

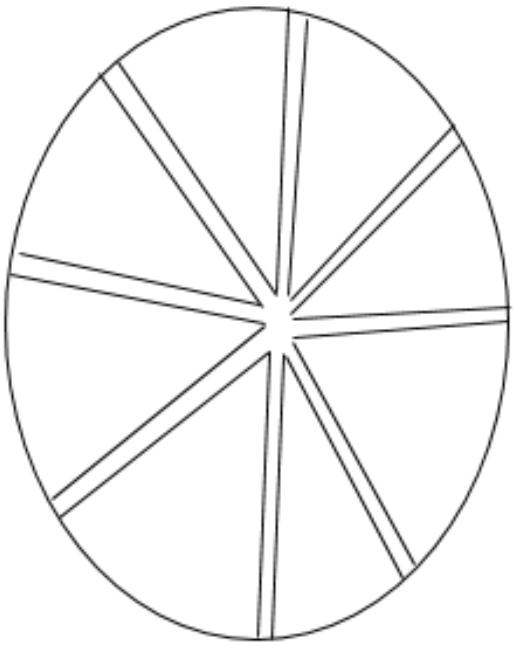

Fig. 6.2. The structure of the device

A layer of gold is either sputtered or electro plated for uniform distribution along the chip. The chip is lastly patterned using a solution of H3PO4:CH3COOH:H2O in a 1:1:150 ratio [87]. Figure 6.2 shows the structure of the device.

The transducer is designed in such a way that it has two transducers placed in concentric circles in the form of eight fingers with some finger space in between. One of the transducers acts as an input source and the other acts as an output source. The transducers used in this model are the IDTs (interdigital transducers). IDTs are three port devices built with electrodes having one electric port and two acoustic ports. If we give input to an electric port, the other two ports generates surface acoustic waves. If one of the acoustic ports is given input, an electric signal and an acoustic wave will be generated [88]. When an electric voltage is applied, it generates an electric field and the generated waves are received by the receiver. The difference in the electric field between the adjacent electrodes converts the input signal into acoustic waves

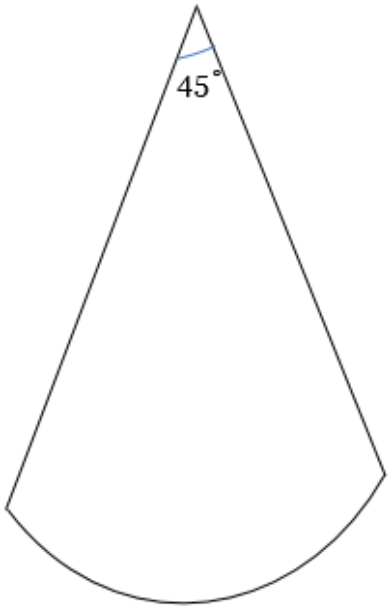

Fig. 6.3. A part of transducer and it's dimensions

and the vice versa happens at the output [88]. According to the designed model the radius of the transducer should be 58.6 mm and the length of the arc should be 46.01mm.

The propagation of the surface waves depends on the thickness of the piezoelectric layer. The ideal thickness for ZnO was found to be 6 micro meters [89]. To arrive at a proper resonating frequency the finger space should half the resonating wavelength λ. Changing the number of finger pairs do not change the sensitivity of the device but using 16 fingers lead to crosstalk between the resonators hence 8 fingers are suggested. The acoustic wave travels through the piezo electric material to a distance equal to 1.5 times the focal length. This sets a delay line of 500 micro meters hence an elliptical structure instead of circular is suggested.

6.3.3 Transducer that Shuts off after Heating up the Fat

This design involves placing a thermal sensor on a micro machined plate through which a substrate is connected via bridge arms. The micro machined plate and bridge arms form the membrane layer having the sacrificial polyimide layer underneath [90]. A half wheat stone bridge is formed by depositing the piezo resistors and by patterning the bridged arms. These are later interconnected through the aluminum. Two bridge serves as the bridge for thermal sensor interconnects while the other half is used to house the piezo resistors [90]. Considering a six arm piezo resistor four of the arms have piezo resistors on them while the other two have titanium interconnects. Six different materials can be used to design this model with silicon nitride as the membrane layer and polysilicon as the piezo resistive layer. For the thermal sensor yttrium barium copper oxide [91-93], gold, titanium can be used. Aluminum layer can be used as metallization layer for connecting the wheat stone bridge resistors acting as pressure sensor. Polys ilicon can be used as the piezo resistor material as it has high strain gauge values [91-93].

6.4 Acoustic Sensor for 0.5Mpas Pressure Detection

The device consists of a saw device that is heated and suspended due to its temperature sensitivity. The device is made pressure sensitive by choosing a proper saw material and also by increasing the operating frequency. The concepts of thermodynamics and gas kinetic theory explains the working of the device. The temperature of the system is said to be in equilibrium when the induced power due to heating is equal to the conducting gas and the power dissipated due to radiation into the surroundings. The change in the pressure induces the change in power due to conduction and this change can be compensated by varying the power that is dissipated due to radiation. And this leads to a variation in device temperature from T_{eq} to T_{f} (final equilibrium) and this change can be expressed by

$$\Delta T = \sqrt[4]{\frac{\psi(T_0 - T_{\text{eq}})\Delta P}{\epsilon\sigma} - T_{\text{eq}}} \tag{6.1}$$

Where ΔP is the change in pressure,T_0 is the temperature of the gas, ϵ is the emissivity of the substrate σ is the Stephans constant and ψ is given by

$$\psi = \frac{\frac{3}{2k}}{\sqrt[2]{2\pi.mkT_0}} \tag{6.2}$$

Where k is the Boltzmann constant and m is the mass of one gas molecule.
The heating resistor of the device is made up of a delay line surrounded by gold or platinum film. The structure is then deposited on a piezoelectric dye and is suspended completely with the wire bonding for providing it with thermal insulation. IDTs of the saw device are connected to the PCB, heater and RF (SMA connector) through wires. The electric current needed for heating the device can be varied by changing the number of wires used for connecting, this increases the thermal conduction between the saw device and the PCB. RF signal is transmitted via PCB, SMA and coaxial connector.

6.4.1 IR Sensor for Temperature Detection

A temperature sensor-RTD manufactured by Honeywell sensing and productivity solutions with the part number HRTS-5760-B-U-0-12 packaged as a probe is highly recommended to be used for this device. It can detect temperature around 0.5° K with an accuracy of 0.5° C. This device has a tolerance rate of 0.1. The device is very actively available.

6.5 The Processing Unit

The output from the transducer is sent to the amplifier to the charge amplifier. From which the output is fed to a low pass filter in order to remove the noise from

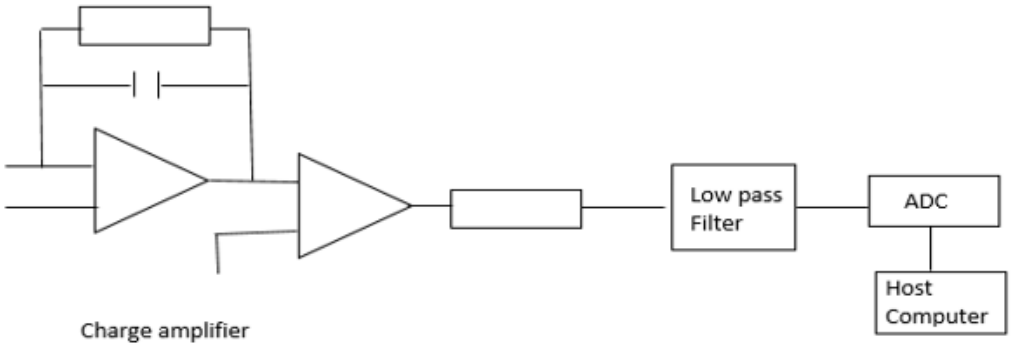

Fig. 6.4. Processing unit

the signals. And then the signals are sent to an ADC. The signals from the ADC are fed to the oscilloscope. Figure 6.4 shows the block diagram of the processing unit.

REFERENCES

REFERENCES

[1] D. Steinberg, "Thematic review series: the pathogenesis of atherosclerosis. an interpretive history of the cholesterol controversy: part ii: the early evidence linking hypercholesterolemia to coronary disease in humans," *Journal of lipid research*, vol. 46, no. 2, pp. 179–190, 2005.

[2] P. Libby, M. Aikawa, and U. Schönbeck, "Cholesterol and atherosclerosis," *Biochimica et Biophysica Acta (BBA)-Molecular and Cell Biology of Lipids*, vol. 1529, no. 1, pp. 299–309, 2000.

[3] A. Nair, B. D. Kuban, E. M. Tuzcu, P. Schoenhagen, S. E. Nissen, and D. G. Vince, "Coronary plaque classification with intravascular ultrasound radiofrequency data analysis," *Circulation*, vol. 106, no. 17, pp. 2200–2206, 2002.

[4] M. Okubo, M. Kawasaki, Y. Ishihara, U. Takeyama, T. Kubota, T. Yamaki, S. Ojio, K. Nishigaki, G. Takemura, M. Saio *et al.*, "Development of integrated backscatter intravascular ultrasound for tissue characterization of coronary plaques," *Ultrasound in medicine & biology*, vol. 34, no. 4, pp. 655–663, 2008.

[5] M. A. Calfon, C. Vinegoni, V. Ntziachristos, and F. A. Jaffer, "Intravascular near-infrared fluorescence molecular imaging of atherosclerosis: toward coronary arterial visualization of biologically high-risk plaques," *Journal of biomedical optics*, vol. 15, no. 1, pp. 011 107–011 107, 2010.

[6] R. I. Levy, R. Lees, and D. Fredrickson, "The nature of pre beta (very low density) lipoproteins." *Journal of Clinical Investigation*, vol. 45, no. 1, p. 63, 1966.

[7] M. Kawasaki, H. Takatsu, T. Noda, K. Sano, Y. Ito, K. Hayakawa, K. Tsuchiya, M. Arai, K. Nishigaki, G. Takemura *et al.*, "In vivo quantitative tissue characterization of human coronary arterial plaques by use of integrated backscatter intravascular ultrasound and comparison with angioscopic findings," *Circulation*, vol. 105, no. 21, pp. 2487–2492, 2002.

[8] Y. Sun, A. J. Chaudhari, M. Lam, H. Xie, D. R. Yankelevich, J. Phipps, J. Liu, M. C. Fishbein, J. M. Cannata, K. K. Shung *et al.*, "Multimodal characterization of compositional, structural and functional features of human atherosclerotic plaques," *Biomedical optics express*, vol. 2, no. 8, pp. 2288–2298, 2011.

[9] F. A. Jaffer, P. Libby, and R. Weissleder, "Optical and multimodality molecular imaging," *Arteriosclerosis, thrombosis, and vascular biology*, vol. 29, no. 7, pp. 1017–1024, 2009.

[10] H. M. Garcia-Garcia, M. A. Costa, and P. W. Serruys, "Imaging of coronary atherosclerosis: intravascular ultrasound," *European heart journal*, vol. 31, no. 20, pp. 2456–2469, 2010.

[11] M. Nauck, G. R. Warnick, and N. Rifai, "Methods for measurement of ldl-cholesterol: a critical assessment of direct measurement by homogeneous assays versus calculation," *Clinical chemistry*, vol. 48, no. 2, pp. 236–254, 2002.

[12] M. Utsunomiya, H. Hara, M. Moroi, K. Sugi, and M. Nakamura, "Relationship between tissue characterization with 40mhz intravascular ultrasound imaging and 64-slice computed tomography," *Journal of cardiology*, vol. 57, no. 3, pp. 297–302, 2011.

[13] T. Araki, M. Nakamura, M. Utsunomiya, and K. Sugi, "Visualization of coronary plaque in type 2 diabetes mellitus patients using a new 40mhz intravascular ultrasound imaging system," *Journal of cardiology*, vol. 59, no. 1, pp. 42–49, 2012.

[14] H. Ma, "Cholesterol and human health," *Nature and Science*, vol. 2, no. 4, 2004.

[15] F. Lindgren, L. Jensen, and F. Hatch, "The isolation and quantitative analysis of serum lipoproteins," *Blood lipids and lipoproteins: quantitation, composition and metabolism*, pp. 181–274, 1972.

[16] R. J. Havel, H. A. Eder, and J. H. Bragdon, "The distribution and chemical composition of ultracentrifugally separated lipoproteins in human serum," *Journal of Clinical Investigation*, vol. 34, no. 9, p. 1345, 1955.

[17] R. Lees and D. Fredrickson, "The differentiation of exogenous and endogenous hyperlipemia by paper electrophoresis." *Journal of Clinical Investigation*, vol. 44, no. 12, p. 1968, 1965.

[18] S. A. Cobb and J. L. Sanders, "Enzymic determination of cholesterol in serum lipoproteins separated by electrophoresis." *Clinical chemistry*, vol. 24, no. 7, pp. 1116–1120, 1978.

[19] N. Muniz, "Measurement of plasma lipoproteins by electrophoresis on polyacrylamide gel." *Clinical chemistry*, vol. 23, no. 10, pp. 1826–1833, 1977.

[20] D. Seidel, H. Wieland, and C. Ruppert, "Improved techniques for assessment of plasma lipoprotein patterns. i. precipitation in gels after electrophoresis with polyanionic compounds," *Clinical chemistry*, vol. 19, no. 7, pp. 737–739, 1973.

[21] W. Neubeck, H. Wieland, A. Habenicht, P. Müller, G. Baggio, and D. Seidel, "Improved assessment of plasma lipoprotein patterns. iii. direct measurement of lipoproteins after gel-electrophoresis." *Clinical chemistry*, vol. 23, no. 7, pp. 1296–1300, 1977.

[22] H. Wieland and D. Seidel, "Fortschritte in der analytik des lipoproteinmusters," *Inn Med*, vol. 5, no. 7, pp. 290–300, 1978.

[23] G. Hoffmann, E. Schleicher, L. Weiss, and S. Hoffmann, "Comparison of two methods for very low density and low density lipoprotein cholesterol determination," *Clinical Chemistry and Laboratory Medicine*, vol. 20, no. 6, pp. 457–460, 1982.

[24] M. Bartholome, H. Wieland, and D. Seidel, "Quantification of plasma lipoprotein cholesterol: a simple procedure for enzymatic determination of cholesterol in electrophoretically separated lipoproteins," *Clinica Chimica Acta*, vol. 104, no. 1, pp. 101–105, 1980.

[25] T. Gordon, W. P. Castelli, M. C. Hjortland, W. B. Kannel, and T. R. Dawber, "High density lipoprotein as a protective factor against coronary heart disease: the framingham study," *The American journal of medicine*, vol. 62, no. 5, pp. 707–714, 1977.

[26] M. Ne, F. Oh, and T. DS, "The tromso heart-study: high-density lipoprotein and coronary heart-disease: a prospective case-control study." *Lancet*, vol. 1, no. 8019, pp. 965–968, 1977.

[27] U. Goldbourt and J. H. MEDALIE, "High density lipoprotein cholesterol and incidence of coronary heart disease the israeli ischemic heart disease study," *American Journal of Epidemiology*, vol. 109, no. 3, pp. 296–308, 1979.

[28] A. Keys, "Alpha lipoprotein (hdl) cholesterol in the serum and the risk of coronary heart disease and death," *The Lancet*, vol. 316, no. 8195, pp. 603–606, 1980.

[29] S. C. Enger, I. Hjermann, O. Foss, A. Helgeland, I. Holme, P. Leren, and K. Norum, "High density lipoprotein cholesterol and myocardial infarction or sudden coronary death: a prospective case-control study in middle-aged men of the oslo study." *Artery*, vol. 5, no. 2, pp. 170–181, 1979.

[30] A. Keys, M. J. Karvonen, S. Punsar, A. Menotti, F. Fidanza, and G. Farchi, "Hdl serum cholesterol and 24–year mortality of men in finland," *International journal of epidemiology*, vol. 13, no. 4, pp. 428–435, 1984.

[31] U. Goldbourt, E. Holtzman, and H. Neufeld, "Total and high density lipoprotein cholesterol in the serum and risk of mortality: evidence of a threshold effect." *Br Med J (Clin Res Ed)*, vol. 290, no. 6477, pp. 1239–1243, 1985.

[32] D. Jacobs, "High-density lipoprotein-cholesterol (hdl-c) and coronary heart-disease (chd), cardiovascular-disease (cvd) and all cause mortality," in *Circulation*, vol. 72, no. 4. Amer Heart Assoc 7272 greenville avenue, Dallax, TX 75231-4596, 1985, pp. 185–185.

[33] S. Pocock, A. Shaper, A. Phillips, M. Walker, and T. Whitehead, "High density lipoprotein cholesterol is not a major risk factor for ischaemic heart disease in british men." *Br Med J (Clin Res Ed)*, vol. 292, no. 6519, pp. 515–519, 1986.

[34] L. O. Watkins, J. D. Neaton, L. H. Kuller, and T. M. R. Groupabc, "Racial differences in high-density lipoprotein cholesterol and coronary heart disease incidence in the usual-care group of the multiple risk factor intervention trial," *The American journal of cardiology*, vol. 57, no. 8, pp. 538–545, 1986.

[35] W. P. Castelli, R. J. Garrison, P. W. Wilson, R. D. Abbott, S. Kalousdian, and W. B. Kannel, "Incidence of coronary heart disease and lipoprotein cholesterol levels: the framingham study," *Jama*, vol. 256, no. 20, pp. 2835–2838, 1986.

[36] D. J. Gordon, J. Knoke, J. L. Probstfield, R. Superko, and H. A. Tyroler, "High-density lipoprotein cholesterol and coronary heart disease in hypercholesterolemic men: the lipid research clinics coronary primary prevention trial." *Circulation*, vol. 74, no. 6, pp. 1217–1225, 1986.

[37] V. Rao and R. Kiran, "Evaluation of correlation between oxidative stress and abnormal lipid profile in coronary artery disease," *Journal of cardiovascular disease research*, vol. 2, no. 1, pp. 57–60, 2011.

[38] N. C. Giehl, "Interference of a homogeneous test for ldl cholesterol by lipoprotein-x," *Clinical Chemistry and laboratory medicine*, 2012.

[39] G. R. Warnick, M. Nauck, and N. Rifai, "Evolution of methods for measurement of hdl-cholesterol: from ultracentrifugation to homogeneous assays," *Clinical Chemistry*, vol. 47, no. 9, pp. 1579–1596, 2001.

[40] S. M. Marcovina, M. L. Koschinsky, J. J. Albers, and S. Skarlatos, "Report of the national heart, lung, and blood institute workshop on lipoprotein (a) and cardiovascular disease: recent advances and future directions," *Clinical chemistry*, vol. 49, no. 11, pp. 1785–1796, 2003.

[41] M. Dashti, W. Kulik, F. Hoek, E. C. Veerman, M. P. Peppelenbosch, and F. Rezaee, "A phospholipidomic analysis of all defined human plasma lipoproteins," *Scientific reports*, vol. 1, p. 139, 2011.

[42] M. Dashty, M. M. Motazacker, J. Levels, M. de Vries, M. Mahmoudi, M. P. Peppelenbosch, F. Rezaee *et al.*, "Proteome of human plasma very low-density lipoprotein and low-density lipoprotein exhibits a link with coagulation and lipid metabolism," *Thrombosis and haemostasis*, vol. 111, no. 3, pp. 518–530, 2014.

[43] J. P. Segrest, M. K. Jones, H. De Loof, and N. Dashti, "Structure of apolipoprotein b-100 in low density lipoproteins," *Journal of lipid research*, vol. 42, no. 9, pp. 1346–1367, 2001.

[44] M. F. Lopes-Virella, P. Stone, S. Ellis, and J. A. Colwell, "Cholesterol determination in high-density lipoproteins separated by three different methods." *Clinical chemistry*, vol. 23, no. 5, pp. 882–884, 1977.

[45] N. C. Bhalodkar, S. Blum, T. Rana, R. Kitchappa, A. N. Bhalodkar, and E. A. Enas, "Comparison of high-density and low-density lipoprotein cholesterol subclasses and sizes in asian indian women with caucasian women from the framingham offspring study," *Clinical cardiology*, vol. 28, no. 5, pp. 247–251, 2005.

[46] G. R. Warnick, R. H. Knopp, V. Fitzpatrick, and L. Branson, "Estimating low-density lipoprotein cholesterol by the friedewald equation is adequate for classifying patients on the basis of nationally recommended cutpoints." *Clinical Chemistry*, vol. 36, no. 1, pp. 15–19, 1990.

[47] W. T. Friedewald, R. I. Levy, and D. S. Fredrickson, "Estimation of the concentration of low-density lipoprotein cholesterol in plasma, without use of the preparative ultracentrifuge," *Clinical chemistry*, vol. 18, no. 6, pp. 499–502, 1972.

[48] D. Kari Gondeck, "Ldl particle number and size," *Advance for NPs and PAs*, 2012.

[49] V. G. Andreev, A. A. Karabutov, S. V. Solomatin, E. V. Savateeva, V. Aleynikov, Y. V. Zhulina, R. D. Fleming, and A. A. Oraevsky, "Optoacoustic tomography of breast cancer with arc-array transducer," in *Proc. SPIE*, vol. 3916, no. 36-47, 2000, pp. 0277–786X.

[50] A. A. Oraevsky, A. A. Karabutov, S. V. Solomatin, E. V. Savateeva, V. A. Andreev, Z. Gatalica, H. Singh, and R. D. Fleming, "Laser optoacoustic imaging of breast cancer in vivo," in *Proc. SPIE*, vol. 4256, no. 6.15, 2001.

[51] A. A. Oraevsky, E. V. Savateeva, S. V. Solomatin, A. A. Karabutov, V. G. Andreev, Z. Gatalica, T. Khamapirad, and P. M. Henrichs, "Optoacoustic imaging of blood for visualization and diagnostics of breast cancer," in *Proc. SPIE*, vol. 4618, no. 10, 2002, pp. 81–94.

[52] P.-C. Li, C.-R. C. Wang, D.-B. Shieh, C.-W. Wei, C.-K. Liao, C. Poe, S. Jhan, A.-A. Ding, and Y.-N. Wu, "In vivo photoacoustic molecular imaging with simultaneous multiple selective targeting using antibody-conjugated gold nanorods," *Optics Express*, vol. 16, no. 23, pp. 18 605–18 615, 2008.

[53] E. Z. Zhang and P. C. Beard, "Ultrahigh-sensitivity wideband fabry-perot ultrasound sensors as an alternative to piezoelectric pvdf transducers for biomedical photoacoustic detection," in *Proceedings of SPIE*, vol. 5320, 2004, pp. 222–229.

[54] G. Ku, X. Wang, G. Stoica, and L. V. Wang, "Multiple-bandwidth photoacoustic tomography," *Physics in medicine and biology*, vol. 49, no. 7, p. 1329, 2004.

[55] F. Duck, "Physical properties of tissue (Academic, London)," 1990.

[56] M. Xu and L. V. Wang, "Photoacoustic imaging in biomedicine," *Review of scientific instruments*, vol. 77, no. 4, p. 041101, 2006.

[57] Z. ANSI, "136.1 american national standard for safe use of lasers," *Laser Institute of America, Orlando*, 2000.

[58] K. Maslov and L. V. Wang, "Photoacoustic imaging of biological tissue with intensity-modulated continuous-wave laser," *Journal of biomedical optics*, vol. 13, no. 2, pp. 024 006–024 006, 2008.

[59] C. Patel and A. Tam, "Pulsed optoacoustic spectroscopy of condensed matter," *Reviews of Modern Physics*, vol. 53, no. 3, p. 517, 1981.

[60] Z. Yu, J. Assif, G. Magoon, P. Kebabian, W. Brown, W. Rundgren, J. Peck, R. Miake-Lye, D. Liscinsky, and B. True, "Differential photoacoustic spectroscopic (dpas)-based technique for pm optical absorption measurements in the presence of light absorbing gaseous species," *Aerosol Science and Technology*, pp. 1–10, 2017.

[61] C. G. Hoelen and F. F. de Mul, "Image reconstruction for photoacoustic scanning of tissue structures," *Applied Optics*, vol. 39, no. 31, pp. 5872–5883, 2000.

[62] A. C. Tam, "Applications of photoacoustic sensing techniques," *Reviews of Modern Physics*, vol. 58, no. 2, p. 381, 1986.

[63] M. W. Sigrist, "Laser generation of acoustic waves in liquids and gases," *Journal of applied physics*, vol. 60, no. 7, pp. R83–R122, 1986.

[64] W.-F. Cheong, S. A. Prahl, and A. J. Welch, "A review of the optical properties of biological tissues," *IEEE journal of quantum electronics*, vol. 26, no. 12, pp. 2166–2185, 1990.

[65] J. Mobley, "Optical properties of tissue," *Biomedical photonics handbook*, pp. 20–95, 2003.

[66] K. R. Foster, "Thermal and nonthermal mechanisms of interaction of radio-frequency energy with biological systems," *IEEE Transactions on Plasma Science*, vol. 28, no. 1, pp. 15–23, 2000.

[67] C. C. Johnson and A. W. Guy, "Nonionizing electromagnetic wave effects in biological materials and systems," *Proceedings of the IEEE*, vol. 60, no. 6, pp. 692–718, 1972.

[68] V. E. Gusev and A. A. Karabutov, "Laser optoacoustics," *NASA STI/Recon Technical Report A*, vol. 93, 1991.

[69] B. J. Vakoc, G. J. Tearney, and B. E. Bouma, "Real-time microscopic visualization of tissue response to laser thermal therapy," *Journal of Biomedical Optics*, vol. 12, no. 2, pp. 020 501–020 501, 2007.

[70] T. Vo-Dinh, *Biomedical photonics handbook: biomedical diagnostics*. CRC press, 2014.

[71] G. Ku and L. V. Wang, "Scanning thermoacoustic tomography in biological tissue," *Medical physics*, vol. 27, no. 5, pp. 1195–1202, 2000.

[72] G. Ku and L. V. Wang, "Scanning microwave-induced thermoacoustic tomography: Signal, resolution, and contrast," *Medical Physics*, vol. 28, no. 1, pp. 4–10, 2001.

[73] L. Wang, "Scanning microwave induced acoustic tomography," Texas Engineering Experiment Station College Station, Tech. Rep., 2004.

[74] R. A. Kruger and P. Liu, "Photoacoustic ultrasound: Pulse production and detection in 0.5% liposyn," *Medical physics*, vol. 21, no. 7, pp. 1179–1184, 1994.

[75] C.-W. Chan and P. Cawley, "Guided waves for the detection of defects in welds in plastic pipes," in *Review of progress in quantitative nondestructive evaluation*. Springer, 1995, pp. 1537–1544.

[76] J. Zhu, *Optimization of matching layer design for medical ultrasonic transducer*. The Pennsylvania State University, 2008.

[77] H. Huisman, "Diagnostic ultrasound: Physics and equipment: Pr hoskins, a. thrush, k. martin, ta wittingham, greenwich medical media ltd., 2003, 233 pp." 2004.

[78] K. K. Shung and M. Zippuro, "Ultrasonic transducers and arrays," *IEEE Engineering in Medicine and Biology Magazine*, vol. 15, no. 6, pp. 20–30, 1996.

[79] S. Xiang and Y. Zhang, "Matching layer optimization between ultrasound transducer and human tissues," in *Engineering in Medicine and Biology Society, 1995., IEEE 17th Annual Conference*, vol. 1. IEEE, 1995, pp. 623–624.

[80] T. G. Álvarez-Arenas, "Acoustic impedance matching of piezoelectric transducers to the air," *IEEE transactions on ultrasonics, ferroelectrics, and frequency control*, vol. 51, no. 5, pp. 624–633, 2004.

[81] K. Kalantar-Zadeh and W. Wlodarski, "Surface acoustic wave sensor," 11 2006, US Patent 7,027,921.

[82] T. B. Gabrielson, "Mechanical-thermal noise in micromachined acoustic and vibration sensors," *IEEE transactions on Electron Devices*, vol. 40, no. 5, pp. 903–909, 1993.

[83] L. G. L. C. B. Zhao and J. P. Yong, "Progress of research on chemical sensing films of surface acoustic wave gas sensor [j]," *Analytical Instrumentation*, vol. 3, p. 003, 2007.

[84] W. König, Y. Altintas, and F. Memis, "Direct adaptive control of plunge grinding process using acoustic emission (ae) sensor," *International Journal of Machine Tools and Manufacture*, vol. 35, no. 10, pp. 1445–1457, 1995.

[85] S. Sathyanarayana, S. Carlier, W. Li, and L. Thomas, "Characterisation of atherosclerotic plaque by spectral similarity of radiofrequency intravascular ultrasound signals," *EuroIntervention*, vol. 5, no. 1, pp. 133–139, 2009.

[86] P. Nicolay, O. Elmazria, F. Sarry, L. Bouvot, N. Marche, and H. Kambara, "Innovative surface acoustic wave sensor for accurate measurement of subatmospheric pressure," *Applied Physics Letters*, vol. 92, no. 14, p. 141909, 2008.

[87] P. Nicolay, O. Elmazria, F. Sarry, L. Bouvot, H. Kambara, K. J. Singh, and P. Alnot, "Wide vacuum pressure range monitoring by pirani saw sensor," *IEEE transactions on ultrasonics, ferroelectrics, and frequency control*, vol. 57, no. 3, 2010.

[88] V. Shamanna, S. Das, Z. Çelik-Butler, D. P. Butler, and K. L. Lawrence, "Micromachined integrated pressure–thermal sensors on flexible substrates," *Journal of Micromechanics and Microengineering*, vol. 16, no. 10, p. 1984, 2006.

[89] C. M. Travers, A. Jahanzeb, D. P. Butler, and Z. Celik-Butler, "Fabrication of semiconducting ybacuo surface-micromachined bolometer arrays," *Journal of microelectromechanical systems*, vol. 6, no. 3, pp. 271–276, 1997.

[90] A. Jahanzeb, C. M. Travers, Z. Celik-Butler, D. P. Butler, and S. G. Tan, "A semiconductor ybacuo microbolometer for room temperature ir imaging," *IEEE transactions on electron devices*, vol. 44, no. 10, pp. 1795–1801, 1997.

[91] J. E. Gray, Z. Celik-Butler, and D. P. Butler, "Mgo sacrificial layer for micromachining uncooled y-ba-cu-o ir microbolometers on si/sub 3/n/sub 4/bridges," *Journal of microelectromechanical systems*, vol. 8, no. 2, pp. 192–199, 1999.

[92] P. French and A. Evans, "Piezoresistance in polysilicon and its applications to strain gauges," *Solid-State Electronics*, vol. 32, no. 1, pp. 1–10, 1989.

[93] P. Clerc, L. Dellmann, F. Gretillat, M. Gretillat, P. Indermühle, S. Jeanneret, P. Luginbuhl, C. Marxer, T. Pfeffer, G. Racine *et al.*, "Advanced deep reactive ion etching: a versatile tool for microelectromechanical systems," *Journal of Micromechanics and Microengineering*, vol. 8, no. 4, p. 272, 1998.

APPENDICES

A. DEMONSTRATE CITATIONS

[1] [2] [3] [4] [5] [6] [7] [8] [9] [10] [11] [12] [13] [14] [15] [16] [17] [18] [19] [20] [21] [22] [23] [24] [25] [26] [27] [28] [29] [30] [31] [32] [33] [34] [35] [36] [37] [38] [39] [40] [41] [42] [43] [44] [45] [46] [47] [48] [49] [50] [51] [52] [53] [54] [55] [56] [57] [58]

[59] [60] [61]

[62] [63] [55] [64] [64] [65] [66] [67] [68] [69] [70] [71] [72] [73] [74] [75] [76] [77] [78] [79] [80] [76] [81] [82] [83] [84] [5] [7] [85] [9] [86] [87] [88] [89] [90] [91] [92] [93]